NEURAL REGENERATION RESEARCH
www.nrronline.org

Research Article

ADAM10 facilitates rapid neural stem cell cycling and proper positioning within the subventricular zone niche via JAMC/RAP1Gap signaling

https://doi.org/10.4103/1673-5374.339007

Date of submission: May 17, 2021

Date of decision: July 1, 2021

Date of acceptance: August 4, 2021

Date of web publication: April 1, 2022

Nadia McMillan[1, 2, 3], Gregory W. Kirschen[4], Sanket Desai[2], Emma Xia[2], Stella E. Tsirka[2, *, #], Adan Aguirre[2, #]

From the Contents

Introduction	2472
Materials and Methods	2473
Results	2475
Discussion	2481

Graphical Abstract *ADAM10 cleaves JAMC to increase RAP1GAP activity, promoting neural stem cell cycling and apical-to-basal translocation in the SVZ stem cell niche*

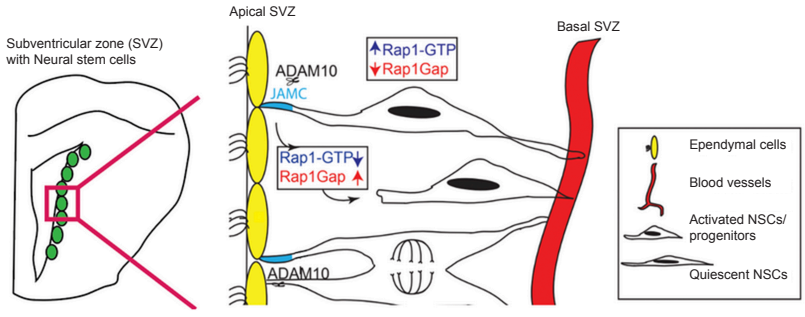

Abstract

The mechanisms that regulate neural stem cell (NSC) lineage progression and maintain NSCs within different domains of the adult neural stem cell niche, the subventricular zone are not well defined. Quiescent NSCs are arranged at the apical ventricular wall, while mitotically activated NSCs are found in the basal, vascular region of the subventricular zone. Here, we found that ADAM10 (a disintegrin and metalloproteinase 10) is essential in NSC association with the ventricular wall, and via this adhesion to the apical domain, ADAM10 regulates the switch from quiescent and undifferentiated NSC to an actively proliferative and differentiating cell state. Processing of JAMC (junctional adhesion molecule C) by ADAM10 increases Rap1GAP activity. This molecular machinery promotes NSC transit from the apical to the basal compartment and subsequent lineage progression. Understanding the molecular mechanisms responsible for regulating the proper positioning of NSCs within the subventricular zone niche and lineage progression of NSCs could provide new targets for drug development to enhance the regenerative properties of neural tissue.

Key Words: ADAM10; adhesion; junctional adhesion molecule C; neural stem cells; neurogenesis; olfactory bulb; Rap1Gap; sub-ventricular zone

Introduction

In adult tissue, specific stem cells reside within specialized microenvironments termed "niches" that control stem cell behavior. Important questions are aimed at both determining the characteristics of the niche that can maintain cells in an undifferentiated state, and how neural stem cells (NSCs) respond to pathologic brain insults. Knowledge of NSC participation in regeneration can help develop therapeutic strategies to enhance repair effects. The subventricular zone (SVZ) is a specialized microenvironment in the central nervous system (CNS) that provides necessary signaling elements for maintaining NSC behavior (Doetsch et al., 1999). The niche is composed of distinct cell types: ependymal cells, NSCs and their progeny, transit-amplifying cells, and neuroblasts. The majority of quiescent NSCs maintain unique pinwheel architecture. The pinwheel's core contains the apical endings of B1 cells and in its periphery two types of ependymal cells: E1 multi-ciliated and E2 cells with only 2 cilia and complex basal bodies (Cheung and Rando, 2013). In addition to the cellular entities, the SVZ consists of a rich vascular network and an elaborate configuration of extracellular matrix components (ECM) that, as a whole, are necessary for the preservation of stemness throughout life (Lathia et al., 2007; Loulier et al., 2009; Fuentealba et al., 2012; Gattazzo et al., 2014). The adult SVZ microenvironment is organized in two critical compartments referred to as the apical and basal niches (Fuentealba et al., 2012). The apical compartment is found adjacent to the ventricular wall while the basal compartment contains a vascular network. In this context, quiescent NSCs are arranged at the ventricular wall, while mitotically activated NSCs are found adjacent to the basal, vascular region of the SVZ. Although the elements that constitute and maintain the basal and apical niches are well understood (Shen et al., 2008; Kokovay et al., 2012), there is a gap in the understanding of signaling cues that regulate NSC positioning and transit between different compartments. Expression levels of extracellular matrix and adhesion molecules that direct NSC-NSC and NSC-niche interactions are tightly regulated and appear to correlate with NSC positioning to control cell fate decision between self-renewal and/or lineage progression (Doetsch et al., 2002; Aguirre et al., 2005; Lathia et al., 2007; Loulier et al., 2009; Kokovay et al., 2010, 2012; Porlan et al., 2014). The role of proteases in ECM reorganization and cell surface receptor/ligand regulation has come to light as a means of directing stem cell adhesion, migration, and proliferation of NSCs during development and disease (Aguirre et al., 2005; Reiss et al., 2005; Solanas et al., 2011).

ADAM10 (a disintegrin and metalloproteinase 10) is highly expressed in the CNS, including the SVZ. Its sheddase activity functions to cleave membrane proteins at the cell surface and releases the protein's soluble ectodomain, which is essential both during development and in adult tissue. Interestingly,

[1]Program in Neuroscience and Medical Scientist Training Program, Renaissance School of Medicine at Stony Brook University, Stony Brook, NY, USA; [2]Department of Pharmacological Sciences, Renaissance School of Medicine at Stony Brook University, Stony Brook, NY, USA; [3]Department of Neurology, Beth Israel Deaconess Medical Center/Harvard Medical School, Boston, MA, USA; [4]Department of Gynecology and Obstetrics, Johns Hopkins Hospital, Baltimore, MD, USA

***Correspondence to:** Stella E. Tsirka, PhD, styliani-anna.tsirka@stonybrook.edu.

https://orcid.org/0000-0003-0022-1770 (Stella E. Tsirka)

#These two authors contributed equally to this paper.

Funding: *This work was supported by National Institutes of Health (NIH) Grants R01 RMH099384 (to AA) and T32GM008444 (to NM).*

How to cite this article: *McMillan N, Kirschen GW, Desai S, Xia E, Tsirka SE, Aguirre A (2022) ADAM10 facilitates rapid neural stem cell cycling and proper positioning within the subventricular zone niche via JAMC/RAP1Gap signaling. Neural Regen Res 17(11):2472-2483.*

the human orthologue to the mouse ADAM10 is currently being investigated for its potential role in Alzheimer's disease (Harrison et al., 2021). In the context of stem cell biology, ADAM10 is central in regulating stem cell properties. In the intestinal stem cell niche and mouse spleen, ADAM10 acts cell-autonomously to direct progenitor cell lineage specification (Tsai et al., 2014; Saftig and Lichtenthaler, 2015) and it also promotes epithelial cell sorting and compartmentalization (Solanas et al., 2011). The role of ADAM10 in the shedding of synaptic adhesion protein, NLGN3, and gliomagenesis has recently been reported. Pan et al. (2021) showed that inhibition of ADAM10 by the small molecule GI254023X resulted in decreased growth of optic nerve glioma.

In the context of the CNS, ADAM10 promotes progenitor cell polarization and migration towards sites of white matter injury during demyelination by shedding N-cadherin (Klingener et al., 2014). Each of these studies identified a distinct substrate mediating phenotype downstream of ADAM10. ADAM10 regulates stem cell biology either autonomously by shedding several key signaling elements present in stem cells (Notch, APP, Cadherins, EGFR ligands, junctional adhesion molecules [JAMs] (Wen et al., 1997; Janes et al., 2005; Rabquer et al., 2010; Brennaman et al., 2014; Porlan et al., 2014)) or non-autonomously by regulating the shedding of extracellular signaling elements in the niche (Janes et al., 2005; Chen et al., 2007). Although ADAM10 has been shown to preserve stem cell properties and microenvironments, the role of proteases in the regulation of the position of stem cells in their microenvironment is still largely unknown (Zhang et al., 2020; Zhu et al., 2021).

Of therapeutic interest, recent studies demonstrated that activation and mobilization of endogenous NSCs might be a reliable approach to promoting brain repair. However, the molecular basis of the SVZ niche adapting to instruct NSC remains poorly understood. In this study, we deleted ADAM10 in mouse models to investigate the homeostatic role of ADAM10 in neural stem cell maintenance and regeneration with the expectation that a better understanding will lead to future therapies to promote brain repair.

Materials and Methods

Animals

Animal experiments were performed in accordance with the National Institutes of Health (NIH) Guide for the Care and Use of Laboratory Animals and approved by the Institutional Animal Care and Use Committee of Stony Brook University (Protocol # 246165). Mice were housed in the institutional facility with 12-hour dark/light cycles, room temperature, and free access to food and water. C57BL/6 (wide-type, WT) and transgenic strains backcrossed to C57BL/6 mice were used. The transgenic mouse strains Nestin-Cre^{ER}; ADAM10$^{fl/fl}$/Rosa26YFP and glial fibrillary acidic protein-green fluorescent protein (GFAP-GFP) were previously described (Aguirre et al., 2010; Klingener et al., 2014). Nestin-Cre (stock No. 012906, RRID: IMSR_JAX:012906) was obtained from Jackson Laboratories, Bar Harbor, ME, USA. Mouse genotyping was conducted by PCR amplification of genomic DNA obtained by digesting mouse tail snips in Solution A (25 mM NaOH, 0.2 mM ethylenediaminetetraacetic acid) for 45 minutes at 98°C. The DNA digestion mixture was mixed with an equal amount of Solution B (45 mM Tris-HCl). Mouse DNA was genotyped with the following primers: ADAM10, 5′-CGT ATC TCA AAA CTA CCC TCC C-3′ (forward) and 5′-GTT GGA CAT AAC TTT GGA TCT CC-3′ (reverse); Cre, 5′-GCG GTC TGG CAG TAA AAA CTA TC-3′ (forward) and 5′-CGT TTT CGT TCT GCC AAT ATG G-3′ (reverse); YFP, 5′-GAC GAC GGC AAC TAC AAG AC-3′ and 5′-ATG TGA TCG CGC TTC TCG T-3′ (reverse).

Genomic DNA was mixed with primers and Phusion High-Fidelity PCR Master Mix (New England BioLabs, Ipswich, MA, USA) for genotyping.

RNA isolation for expression analysis

RNA was purified from SVZ or fluorescence-activated cell sorting (FACS)-sorted YFP^{+} populations with the RNeasy Kit (Qiagen, Germantown, MD, USA). cDNA was synthesized with qScript cDNA SuperMix (Quanta BioSciences, Gaithersburg, MD, USA). Primers spanning exons 9–10 to monitor deletion of the protease domain of *ADAM10* are available on request. Gene array was performed by the Stony Brook University Genomic Core with the Affymetrix GeneChip Mouse Genome 430 2.0 Array (data not shown) on WT and ADAM10$^{fl/fl}$ SVZ samples.

Quantitative reverse transcription-polymerase chain reaction

The isolated RNA was separated from the aqueous phase using an RNeasy MicroKit (74004, Qiagen, Germantown, MD, USA). cDNA was reverse transcribed using random primers and Superscript IV (18090200, Thermo Fisher Scientific, Waltham, MA, USA). PCR was performed from cDNA using Phusion Flash High-Fidelity PCR Master Mix (F548L, Thermo Fisher Scientific) as per the manufacturer's protocol on an Applied Biosystems 7900HT real-time PCR system (Ct values above 35 cycles were not considered for the analysis). Fold changes were calculated using the ΔΔCt method. All gene expression levels were normalized to GAPDH mRNA levels.

Tamoxifen and bromodeoxyuridine administration

For induction of recombination, Nestin-Cre^{ER}/ADAM10$^{fl/fl}$ mice (4–6 weeks old) were administered tamoxifen (TAM) at 100 mg/kg per day for 3 days with 48 hours apart (intraperitoneally (IP); dissolved in 10% EtOH/90% sunflower oil). Littermate mice WT for ADAM10 or negative for Nestin-Cre were used as controls and were also treated with tamoxifen concurrent with ADAM10$^{fl/fl}$ mice. For *in vitro* experiments, hydroxy-tamoxifen (4-OHT; MilliporeSigma, Burlington, MA, USA), a TAM metabolite, was added at 1 μM to the stem cell media (SCM; 1:1 DMEM:F12 medium (MilliporeSigma) 1× B27 supplement) for the duration of the experiment unless otherwise indicated.

For the bromodeoxyuridine (BrdU)-label-retaining cell (LRC-BrdU) assay, BrdU (10 mg/mL, MilliporeSigma) was injected IP at 100 mg/kg five times every 3 hours into P45 ADAM10$^{fl/fl}$ and WT control mice following TAM administration to label dividing cells. Mice were euthanized 30 days after the final BrdU injection. *In vitro* short-term BrdU analysis involved BrdU administration (10 μM) 2 hours before fixation.

Acitretin administration

For *in vivo* experiments, mice were injected with Acitretin (5 mg/kg (IP), MilliporeSigma) to increase ADAM10 activity 18 and 4 hours before tissue harvest. *In vitro*, acitretin (10 μM) was added at the same time points. Increased ADAM10 activity in the SVZ was demonstrated following IP injections of acitretin with SensoLyte 520 ADAM10 Activity Assay Kit (AnaSpec, San Jose, CA, USA).

Neurosphere cultures and culture-based assays

Adult SVZ tissue was dissected into the Hanks' Balanced Salt Solution (MilliporeSigma) containing 26 mM (4-(2-hydroxyethyl)-1-piperazineethanesulfonic acid) (HEPES), 0.3% glucose, and 0.75% sucrose (D1 medium). Tissue was dissociated into single-cell suspensions using papain (10 mg/mL), 0.1% trypsin, and 100 U/mL DNase I (MilliporeSigma) in D1 medium for 25 minutes at room temperature. For self-renewal assays, single-cell suspensions were plated in floating cultures at a clonal density in stem-cell medium (SCM [MilliporeSigma]; 1:1 DMEM: F12 medium, 1× B27 supplement, 1% penicillin/streptomycin, epidermal growth factor [EGF, Millipore Bioscience Research Reagents, Burlington, MA, USA, 20 ng/mL], basic fibroblast growth factor [bFGF2, Millipore Bioscience Research Reagents,10 ng/mL]) as previously described (Aguirre et al., 2010). Sphere formation was quantified 7 days after plating. For differentiation experiments, secondary neurospheres were dissociated after 7 days *in vitro* (DIV) using TrypLE (Thermo Fisher Scientific) and single cells were plated onto poly-L-lysine (PLL; 100 μg/mL)-coated coverslips or 6-well plates. These cultures were maintained for 7 DIV in SCM without EGF or fibroblast growth factor and then processed for immunofluorescence analysis with stem cells or neural lineage-specific antibodies. Immunoblotting of differentiated secondary neurospheres was performed similarly but cells were plated in 6-well PLL-coated dishes. All neurosphere, cell, and tissue explant cultures were incubated in a humidified incubator maintained at 37°C and 5% CO_2.

Transfections

pcDNA-JAM3 plasmids were prepared as previously reported (Santoso et al., 2002). pcDNA-dsRED vectors were used as a control to investigate the transfection effects on endogenous gene expression. Transfection was performed using PolyJet (SignaGen Laboratories, Gaithersburg, MD, USA) in a 3:1 ratio as per the manufacturer's instructions.

Lentivirus production

pGFP-C-shLenti expression vectors carrying shRNAs to mJAMC or scrambled controls were purchased from OriGene, Austin, TX, USA. pLOC-GFP-Rap1GAP and control lentivirus were purchased from MilliporeSigma and provided by Lewis Kaufman as previously described (Kerever et al., 2007). Lentivirus was generated using the lentiviral transfer vector co-transfected with the vesicular stomatitis virus G (pCMV-VSV-G) viral envelope and gag-pol (pCMV-dR8.2 dvpr) into HEK293 cells (CLS Cat# 300192/p777_HEK293, RRID: CVCL_0045) using Calcium Phosphate Transfection Kit (Clontech, Mountain View, CA, USA). Growth medium (DMEM + 10% FBS; MilliporeSigma) was added to cells after 12 hours, and the supernatant was harvested 24–72 hours after transfection.

Fluorescence-activated cell sorting

YFP^{+} cells from Nestin-CRE^{ER}/ADAM10$^{fl/fl}$/Rosa26YFP and littermate controls were sorted on a FACStar plus instrument (Beckton Dickinson, Franklin Lakes, NJ, USA). YFP was detected using A490 long-pass filters. Cell aggregates and small debris were excluded on the basis of side scatter (measuring cell granularity) and forward scatter (measuring cell size). Gating parameters were set using positive and negative cell populations to measure background fluorescence. Positive cell populations were either used for cell culture experiments or fixed for immunocytochemistry.

SVZ slice culture/SVZ explant cultures

After adult mice were euthanized, the brains were dissected, washed in Hanks' Balanced Salt Solution, and transferred to fresh ice-cold D1 medium. Then, the brains were sectioned into 200–300 μm-thick coronal sections using a tissue chopper (McIlwain, Lafayette Instruments, Lafayette, IN, USA) before careful dissection of the SVZ. SVZ pieces were transferred to 12-well polycarbonate transwell inserts (0.4 μm-sized pore, Corning Incorporated, Corning, NY, USA) containing peptide hydrogel (BD PuraMatrix, Franklin Lakes, NJ, USA) with the ventricular side facing up. SCM (700 μL) was added to each well and supplemented with growth factors. For analysis of the JAMC cleavage product, 4-hydroxytamoxifen (1 μM) was added along with EGF (20 ng/mL) and fibroblast growth factor (10 ng/mL), both from Millipore Bioscience Research Reagents, for the duration of the experiment (4 DIV). An anti-JAMC antibody (R&D Systems, Minneapolis, MN, USA) to the N-terminal domain was used to detect the extracellular product following acitretin addition on days 3 and 4 *in vitro*.

For cell plating experiments, single cells obtained from YFP-sorted secondary neurospheres were dissociated (4000 cells in 10 µL SCM per explant), gently pipetted onto the surface of SVZ explants, and maintained for 4 DIV before fixation and analysis. Although this assay has previously been used to study chemotaxis (Shen et al., 2008), it is also useful for studying cell-autonomous NSC properties in their native environment (Kokovay et al., 2010).

For RAP1Gap over-expression analysis, cells were infected with control or Rap1Gap lentivirus (Origene, Rockville, MD, USA), maintained in culture for 7 days before dissociation with a trypsin-like recombinant protease cocktail (TrypLE, Thermo Fisher Scientific), and plated as before. A minimum of four slice cultures were analyzed per experiment.

Scratch test/migration assay

Wide-type and ADAM10$^{fl/fl}$ secondary neurospheres grown in the presence of 4-hydroxytamoxifen were plated in 6-well PLL-coated dishes or PLL-coated coverslips and maintained to confluency. In monolayers, a cross was created in the cell layer by scratching a pipette tip across the bottom of the well to create a line followed by a second scratch perpendicular to the first line. The wells were washed to remove detached cells and the cross was imaged using a Zeiss Optical Microscope (Zeiss, Oberkochen, Germany). After 24 hours, the cross was re-imaged to analyze migration by capturing an image at the same spot as time 0. By overlaying images from time 0 to 24 hours, migration of an individual cell from the edge of the scratch was quantified using ImageJ64 line measure tool (National Institutes of Health, Bethesda, MD, USA; Schneider et al., 2012). Experiments were performed by analyzing multiple wells and repeated with three biological replicates.

Short-term adhesion assay

50,000 WT or ADAM10$^{fl/fl}$ neural stem and progenitor cells were incubated with Calcein-AM (Life Technologies, Carlsbad, CA, USA; 4 µg/mL) for 20 minutes at 37°C and 5% CO_2. The fluorescence-labeled cells were incubated with JAMC blocking antibody (0.01 µg/µL, Mouse JAM-C Antibody AF1213, R&D Systems) or IgG control for 45 minutes. The cells were added onto PLL (100 µg/mL)-, laminin (10 µg/mL)-, or fibronectin (1 mg/mL) -coated 96-well plates and allowed to adhere for 20 minutes. Non-adherent calcein-labeled cells were removed by gently washing twice with 1× PBS. Adherent cells were calculated as a percentage of total fluorescence before washing. For adhesion experiments with the RAP1 activator, 8-CPT-2-O-Me-cAMP (60 µM; MilliporeSigma), small molecule ADAM10 inhibitor GI245023X (40 µM, MilliporeSigma), or DMSO control, cells were incubated for 15 minutes. The cells were incubated with the small molecule before addition to PLL, laminin, or fibronectin-coated 96-well plates. Adhesion was calculated as above. Experiments were performed in triplicate and repeated three times.

RAP1 activation assay

The RAP-binding domain of RAL-GDS binds only the active form of RAP1, serving as the basis for the RAP-GTP binding assay (Franke et al., 1997). The levels of active GTP-bound RAP1 were determined using the Active RAP1 Pull-Down and Detection Kit (Thermo Fisher Scientific) according to the manufacturer's instruction using WT and ADAM10$^{fl/fl}$ NSCs cultured in 4-hydroxytamoxifen. For over-expression of JAMC, cells were transfected 48 hours before collection. Lentivirus-mediated RAP1GAP over-expression occurred 7 days following initial transduction. Proteins were analyzed by immunoblotting using the anti-RAP1 antibody provided with the kit (Thermo Fisher Scientific).

Immunohistochemistry

Mice were deeply anesthetized with isoflurane and transcardially perfused with PBS (20 mL), followed by a fixative solution (4% paraformaldehyde; 50 mL). Brains were dissected and post-fixed for 4–24 hours before transferring to the cryoprotective solution (30% sucrose) for at least 24 hours. Tissue sectioning was performed using a Leica (Buffalo Grove, IL, USA) sliding microtome. Brain sections (30–50 µm thick) of the region of interest were collected in 0.1 M PBS. Immunostaining was performed using free-floating coronal or sagittal brain slices blocked in 10% normal goat serum (Thermo Fisher Scientific) containing 0.3–0.5% Triton X-100 and 1% albumin (MilliporeSigma) in 0.1 M PBS for 1 hour at room temperature. Tissue sections were incubated overnight at 4°C in blocking solution containing primary antibodies including the following: rat anti-bromodeoxyuridine (BrdU) OBT0030A (1:500), Accurate Chemical and Scientific Corporation, mouse Becton Dickinson, Clone B44 (1:500); anti-Nestin (Chemicon, 1:250, Clone: 25/Nestin, BD Biosciences, East Rutherford, NJ, USA); anti-glial fibrillary acidic protein (GFAP) (BD Biosciences); anti-Ki67 (Novocastra), anti-epidermal growth factor receptor (EGFR; Abcam), anti-vascular cell adhesion molecule 1 (VCAM1; R&D Systems, Minneapolis, MN, USA), anti-RAP1gap (Abcam), anti-green fluorescent protein (GFP; Aves Labs, Davis, CA, USA), anti-Lex (MMA clone, BD Biosciences), anti-JAMC (goat, R&D Systems; rabbit, Novus Biologicals, Littleton, CO, USA), anti-ADAM10 (rabbit, Abcam; rat, R&D Systems), anti-doublecortin (Abcam), CD133 (eBioScience, San Diego, CA, USA), anti-laminin (MilliporeSigma), anti-Sox2 (Chemicon, Rolling Meadows, IL, USA), and anti-microtubule associated protein 2 (MAP2; Abcam). The appropriate secondary antibodies were purchased from Jackson ImmunoResearch (West Grove, PA, USA) and used at 1:500 dilutions in blocking solution for 1 hour at room temperature (**Table 1**).

For BrdU staining, sections were incubated with 2 N hydrochloric acid (HCl) for 20 minutes at 37°C, then washed with 0.1 M $Na_2B_4O_7$ 2× for 10 minutes before standard staining protocol. Coverglass staining was performed by blocking for 10 minutes before addition of primary antibody mixture for 1 hour at room temperature. Coverglasses were gently washed 3 × 5 minutes before addition of appropriate fluorescent dye-conjugated secondary antibody (1:500) for 1 hour at room temperature. Coverglasses were washed 3 × 5 minutes and incubated with 4′,6-diamidino-2-phenylindole (DAPI) to visualize the cell nuclei before mounting with MOWIOL mounting media (Thermo Fisher Scientific).

Table 1 | **Primary and secondary antibodies used in this study**

Antibody	Source and Cat#	RRID
Chicken polyclonal anti-GFAP	Abcam, ab4674	AB_304558
Mouse monoclonal anti-GFAP (clone 52/GFAP)	BD Biosciences, 610565	AB_396365
Rabbit polyclonal anti-laminin	MilliporeSigma, L9393	AB_477163
Mouse monoclonal anti-β-catenin ((14/β-Catenin)	BD Biosciences, 610153	AB_397555
Rat monoclonal anti- mouseVCAM1	R and D Systems, MAB6434	AB_2214050
Rat monoclonal anti-BrdU, clone BU1/75(ICR1)	Accurate Chemical and Scientific Corporation, OBT0030A	AB_2313756
Mouse monoclonal anti-BrdU, Clone: B44	BD Biosciences, 347580	AB_400326
Goat polyclonal anti-mouse JAMC	R&D Systems, AF1213	AB_2234027
Rabbit polyclonal anti-JAMC	Novus biological, NBP1-92032	AB_11013202
Rat monoclonal anti-CD133	Ebioscience, 14-1331-95	AB_2864986
Mouse monoclonal anti- Nestin, Clone: rat-401	Millipore, MAB353	AB_94911
Mouse monoclonal anti- Nestin, Clone: 25/Nestin	BD Biosciences, 611658	AB_399176
Rabbit polyclonal anti-Sox2	Millipore, AB5603	AB_2286686
Chicken polyclonal anti-MAP2	Abcam, ab5392	AB_2138153
Mouse monoclonal anti-Ki67 (Clone K2)	Novacastra/Leica, NCL-Ki67-MM1	AB_442101
Rabbit polyclonal anti-EGFR	Abcam, ab131498	AB_11156941
Mouse monoclonal anti-Lex, clone MMA	BD Biosciences, 347423	AB_400299
Rat monoclonal anti-ADAM10, clone 139712	R&D Systems, MAB946	AB_2222927
Rabbit polyclonal anti-ADAM10	Abcam, ab1997	AB_302747
Rabbit polyclonal anti-doublecortin	Abcam, ab18723	AB_732011
Rabbit monoclonal [Y135] RAP1GAP	Abcam, ab32119	AB_779061
Chicken polyclonal anti-GFP	Aves Labs	AB_2307313
Fluorescein (FITC)-AffiniPure Goat Anti-Mouse IgG (H+L)	Jackson ImmunoResearch Labs, 115095003	AB_2338589
Cy3-AffiniPure Goat Anti-Mouse IgG (H+L)	Jackson ImmunoResearch Labs, 115-165-003	AB_233868
Alexa Fluor 647-AffiniPure Goat Anti-Mouse IgG (H+L)	Jackson ImmunoResearch Labs, 115-605-003	AB_2338902
Fluorescein (FITC)-AffiniPure Goat Anti-Rabbit IgG (H+L)	Jackson ImmunoResearch Labs, 111-095-003	AB_2337972
Cy3-AffiniPure Goat Anti-Rabbit IgG (H+L)	Jackson ImmunoResearch Labs, 111-165-003	AB_2338000
Alexa Fluor 647-AffiniPure Goat Anti-Rabbit IgG (H+L)	Jackson ImmunoResearch Labs, 111-605-003	AB_2338072
Alexa Fluor 647-AffiniPure Goat Anti-Rat IgG (H+L)	Jackson ImmunoResearch Labs, 112-605-003	AB_2338393
Cy3-AffiniPure Goat Anti-Rat IgG (H+L)	Jackson ImmunoResearch Labs, 112-165-003	AB_2338240
Fluorescein (FITC)-AffiniPure Goat Anti-Rat IgG (H+L)	Jackson ImmunoResearch Labs, 112-095-003	AB_2338189
Goat anti-Chicken IgY (H+L), Alexa Fluor 488	Thermo Fisher Scientific, A-11039	AB_2534096

BrdU: 5-Bromo-2'-dexoyuridine; VCAM1: vascular cell adhesion molecule 1; EGFR: epidermal growth factor receptor; GFAP: glial fibrillary acidic protein; GFP: green fluorescent protein; JAMC: Junctional adhesion molecule-C; MAP2: microtubule-associated protein 2.

SVZ whole mount dissection and staining

SVZ whole mounts of the striatal lateral wall were dissected from adult mice (Lois and Alvarez-Buylla, 1993). A 2–4 mm-long strip of SVZ tissue covering the striatum was dissected from the corpus callosum to the ventral tip of the lateral ventricle in ice-cold PBS. The SVZ whole mounts were fixed in cold 4% paraformaldehyde in 0.1 M PBS overnight, washed with PBS, blocked with 10% normal goat serum in PBS/0.3% Triton X-100 for 60 minutes at room temperature, and then incubated with primary antibodies diluted in blocking buffer for 48 hours at 4°C. Tissues were washed three times with PBS/0.3% Triton for 15 minutes each on a rocker and incubated with appropriate secondary antibodies at room temperature for 1 hour. After washes, DAPI was added, and the whole mounts were transferred to a glass slide and coverslipped with MOWIOL mounting media for confocal imaging. The positioning of NSCs within the SVZ was determined under the microscope. Using a scale bar, the distance from the center of the NSC cell body to the nearest blood vessel or the ventricular wall was visualized by laminin staining. The antibodies used are shown in **Table 1**: GFAP, chicken IgG, 1:500 (Abcam); laminin, rabbit IgG, 1:1000 (MilliporeSigma), β-catenin, mouse IgG1, 1:200 (BD Biosciences); VCAM1, rat IgG, 1:500 (R&D Systems). Primary antibodies were visualized using fluorescent dye-conjugated secondary antibodies (Jackson ImmunoResearch and Thermo Fisher Scientific).

Microscopic analysis and quantification

A confocal laser-scanning microscope TCS-SP5 (Leica DMI6000 B instrument, Buffalo Grove, IL, USA) was used for image localization of FITC (488-nm laser line excitation; 522/35 emission filter), Cy3 (570-nm excitation; 605/32

emission filter), and Cy5 (647 excitation; 680/32 emission filter). Optical sections (*z* ranging from 0.5 to 1 µm) of confocal epifluorescence images were sequentially acquired using 10–63× objectives with Leica LAS AF software. NIH ImageJ software was then used to merge images. Merged images were processed in Photoshop CS4 software (Adobe, San Jose, CA, USA) with minimal manipulations of contrast. Cell counting was performed from each experimental condition and compared with the respective control. Tissue sections containing the SVZ niche region were matched across samples in each experimental condition and compared with their respective control. An average of four sections containing the SVZ niche were used to collect serial confocal images for each condition (n = 3–6) using unbiased stereological morphometric information to obtain an estimate of the total number of cells in question. For cells in monolayer, 5–10 images were taken per condition. For GFAP-GFP cellular distribution from the ventricular wall and blood vessels, the distance from the center of the cell body to the nearest vessel surface or lateral ventricle as demarcated by DAPI staining was measured. An average of 200 cells from three pairs of mice in each 40× z-stack was quantified (Klingener et al., 2014).

Immunoblots and immunoprecipitation

For immunoblotting: SVZ tissue was dissected at the end of the experiments and cells were harvested and used for protein extraction using lysis buffer (50 mM Tris-HCl, pH 7.5, 1 mM EDTA, 1 mM EGTA, 1 mM sodium orthovanadate, 50 mM sodium fluoride, 0.1% 2-mercaptoethanol, 1% Triton X-100, plus protease inhibitor cocktail; MilliporeSigma). Protein concentration was quantified using a standard BCA assay (Pierce, Waltham, MA, USA), and 20–50 µg of protein/lane was loaded on 10% sodium dodecyl sulphate-polyacrylamide gel electrophoresis and transferred to polyvinylidene fluoride membranes (Millipore, Burlington, MA, USA) to perform immunoblot analysis. The membranes were blocked in 2% bovine serum albumin and incubated with primary antibodies overnight at 4°C. Primary antibodies, not listed elsewhere, included anti-N-cadherin (BD Transduction Labs, Franklin Lakes, NJ, USA) and anti-cleaved caspase3 (Santa Cruz Biotechnology, Santa Cruz, CA, USA). Proteins were detected using horseradish peroxidase-conjugated secondary antibody (1:5000; Santa Cruz Biotechnology). Bands were visualized by chemiluminescence (Klingener et al., 2014). Plot data are presented in arbitrary units (AU) after normalizing over actin. ImageJ software was used for quantification.

For immunoprecipitation experiments (Klingener et al., 2014): SVZ tissue was lysed with RIPA buffer. Aliquots of 200 µg (for *in vivo* studies) of protein extracts were incubated with antibodies against JAMC (R&D Systems; 1 µg) and 10 µL of protein-A-conjugated agarose beads (Santa Cruz Biotechnology) for 12–16 hours at 4°C. Proteins associated with JAMC were concentrated by centrifugation at 10,000 × *g* for 3 minutes at 4°C and washed twice with cold RIPA buffer to remove nonspecific binding partners. JAMC complexes were resolved on acrylamide gels and detected as described above. Immunoprecipitation experiments were performed three times with SVZ tissue pooled from three mice for each experiment. Experiments were run with input protein extracts alone as the negative control and protein A/G beads as the positive control.

Behavioral tests

Behavioral testing began 2 weeks following the final TAM administration (3 × 48 hours apart). Three days before the behavioral experiments began, mice were housed singly in the behavioral testing room. 24 hours before behavioral testing, animals were habituated by exposure (10 minutes) to an empty open-field arena to familiarize them with the procedure. Odors were presented by placing an odor stimulus or control odor (mineral oil in water) on a cotton tip suspended from a thin cord above the arena so that the tip was ~8 cm from the floor. A test session consisted of two 5-minute odor presentations of the same odor with a 30 or 60 minutes of interval between presentations. These different intervals were tested in separate sessions spaced at least 24 hours apart with different odors used in each test. Odors and control swabs were randomly placed to control for behaviors related to memory. All test odors were dissolved in water (10^{-3} M solution) and freshly prepared before each experiment. Examples of odors used were isoamyl acetate, citrate, and benzaldehyde. We recorded the time animals spent investigating the swab by defining an equal area directly surrounding the odor or control swab. Mouse tracking was recorded using EthoVision XT9 software (Noldus, Wageningen, Netherlands). A significant decrease in investigation time during the second presentation indicates that mice were able to recognize an odor that had been presented previously.

Statistical analysis

Data are presented as the mean ± standard error of the mean (SEM) and were analyzed by Student's unpaired *t*-test (two groups). Paired *t*-test was used when analyzing fold change (two groups). Two-way or one-way analysis of variance followed by a Tukey's *post hoc* test was employed if comparison was made among more than two groups (Prism 6, GraphPad Software, La Jolla, CA, USA and Mac OS X).

Experiments were completed with at least three biologic replicates unless indicated. All means were derived from independent experiments, but included multiple wells and plates per experiment. $P \leq 0.05$ was considered statistically significant.

Results

ADAM10 maintains NSC lineage progression in the SVZ

To understand the potential function of ADAM10 in NSC anchorage and positioning within the niche, we first characterized its expression *in situ*. Staining for ADAM10 in coronal SVZ sections from WT GFAP$^-$/GFP$^+$ mice confirmed that ADAM10 was also expressed by NSCs (GFAP$^-$/GFP$^+$/ADAM10$^+$; **Figure 1A**), as previously reported (Klingener et al., 2014). To define the spatial relationship of ADAM10 with NSCs in the apical and basal SVZ compartments, we used whole-mount preparations to preserve the three-dimensional contacts. Consistent with our previous report, ADAM10 was expressed by NSCs in the SVZ, however, a unique pattern of expression was observed in the apical niche: ADAM10 was highly enriched in the center of the pinwheels, where NSCs were intercalated within the ependymal layer, suggesting that ADAM10 may have a role in NSC positioning to the apical niche (**Figure 1B**). Considering the expression of ADAM10 at unique sites within the SVZ, we sought to determine the role ADAM10 may play in directing NSC biology by analyzing an inducible Cre mouse line to overcome the embryonic lethality in ADAM10$^{-/-}$ mice (Hartmann et al., 2002; Jorissen et al., 2010). To this end, we crossed NestinCRE^{ER} mice harboring a TAM-inducible gene for *Cre recombinase* under the *Nestin* promoter with *ADAM10* floxed (ADAM10$^{fl/fl}$ or fl/fl) mice to generate Nestin-CRE^{ER}/ADAM10$^{fl/fl}$ transgenic animals in which ADAM10 was ablated by TAM-inducible Cre recombinase specifically in NSCs/NPCs (Klingener et al., 2014). This mouse line also contained a floxed YFP reporter gene in the Rosa26 locus to facilitate the monitoring of recombined NSCs/NPCs and tracking of morphologic changes and NSC progeny following ADAM10 deletion (**Figure 1C**). On postnatal day 45 (P45), mice received three injections of TAM every other day to promote deletion of ADAM10 in the SVZ. Using this TAM schedule, an effective ablation of ADAM10 in NSCs was achieved, detected by reduced *ADAM10* mRNA in SVZ Nestin-YFP$^+$ FAC-sorted cells of the ADAM10$^{fl/fl}$ mice as compared with WT, and by immunoblotting (**Figure 1D**).

We characterized NSCs and their lineage in the SVZ after ADAM10 deletion. Five days after the last TAM injection, decreased density of GFAP$^+$Sox2$^+$ NSCs was observed in the ADAM10$^{fl/fl}$ group (**Figure 1E** and **F**). We questioned whether their progeny would also be affected. We stained for markers of NSCs and NPCs (EGFR, DCX), but since surface expression of these markers rendered it technically difficult to quantify activated NSCs/NPCs *in vivo*, we used acutely dissociated SVZ tissue. The reduction of NSCs in the SVZ was also reflected in the number of lineage cells, as the significantly decreased density of EGFR$^+$ NSCs/NPCs and DCX$^+$ neuroblasts were also detected in acutely dissociated ADAM10$^{fl/fl}$ SVZ tissue (cell counts reported in figure legend; **Figure 1G–I**). To determine whether the decrease in neuroblasts was due to decreased NSC lineage commitment and not a result of progenitor cell death, we administered three injections of TAM every other day to P45 mice (Nestin-CRE^{ER}/ADAM10$^{fl/fl}$/Rosa26YFP) to promote deletion of ADAM10 in the SVZ and analyzed cleaved-caspase 3 levels in cells at P51 prior to cell fate determination (**Figure 1J**). Comparable protein levels were detectable in WT and ADAM10$^{fl/fl}$ cells after the onset of differentiation *in vitro* (**Figure 1K**; P = 0.2622). Thus, deletion of ADAM10 in NSCs led to a decrease in the density of NSCs, NPCs, and neuroblasts without affecting cell death, raising the question of whether ADAM10 alters cell cycle dynamics or dispersion.

ADAM10 regulates the dynamics of NSC cell cycle

The reduced numbers of NSCs and neuroblasts suggest that ADAM10 regulated NSC dispersal; however, it could also have affected the speed of cell cycling. To appreciate NSC turnover, cell cycle dynamics were explored *in vivo* and *in vitro*. First, NSC retention within the SVZ was analyzed after ADAM10 deletion by examining BrdU-LRCs in the SVZ (Johansson et al., 1999a, b). This assay relies on the fact that slowly cycling NSCs retain strong BrdU labeling, whereas in dividing cells the BrdU signal is diluted as the cells leave the niche within the chase period (Johansson et al., 1999a, b). For this experiment, P45 NestinCre^{ER};ADAM10$^{fl/fl}$/Rosa26YFP mice were injected with TAM three times, 48 hours apart, followed by with BrdU five times every 3 hours. Analysis was performed at P75 after a 30 day chase (**Figure 2A**). Significantly more LRC-BrdU$^+$ cells were observed in the WT *versus* ADAM10$^{fl/fl}$ SVZ (**Figure 2B** and **C**). To characterize whether the LRC-BrdU$^+$ cells were stem cells or terminally differentiated cells, LRC-BrdU$^+$ cells were co-immunolabeled with the NSC marker Sox2, as above. Significantly more slowly cycling NSCs were present (LRC-BrdU$^+$Sox2$^+$) in the SVZ of ADAM10$^{fl/fl}$ mice (P = 0.0053; **Figure 2D** and **E**), indicating that ADAM10 deletion results in a more 'quiescent' NSC niche.

Since the increase in slowly cycling LRC-BrdU$^+$ NSCs may imply differences in cell cycle kinetics in the ADAM10$^{fl/fl}$ compared with the WT mice, the impact of ADAM10 deletion on the rate of cell cycle withdrawal was evaluated. An *in vitro* system was then used which allowed for homogenous uptake of BrdU between the two conditions prior to deletion of ADAM10. This approach also allowed for improved analysis of SVZ cells that may leave the niche during the period of ADAM10 deletion and BrdU uptake. BrdU was administered to WT and ADAM10$^{fl/fl}$ NSCs for 24 hours to label cycling cells (S-phase) prior to administering 4-hydroxytamoxifen to delete ADAM10 in floxed cells, followed by growth factor removal (**Figure 2F**). Cells were then analyzed for co-expression with Ki67 to quantify the number of BrdU-labeled cells remaining in the cell cycle: a higher number of cycling stem cells was observed in ADAM10$^{fl/fl}$ (BrdU$^+$Ki67$^+$/total BrdU$^+$ cells) *versus* WT and cells, suggesting an increased probability that the cells remained in the cell cycle rather than exiting the cell cycle (BrdU$^+$Ki67$^-$/total BrdU$^+$; **Figure 2G–I**).

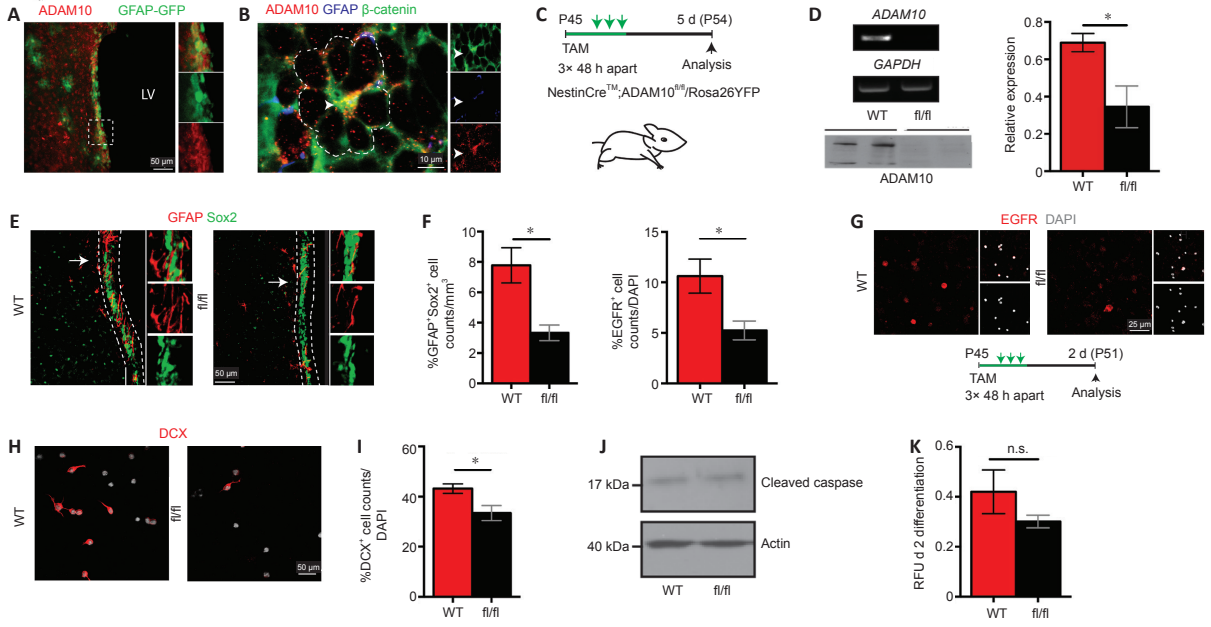

Figure 1 | **GFAP⁺ stem cells in the subventricular zone (SVZ) interact with their niche through ADAM10 initiated contacts.**
(A) Immunostaining for ADAM10 in coronal SVZ sections demonstrates ADAM10 (red) expression in the SVZ co-localizing with GFAP-GFP⁺ (green) neural stem cells (NSCs). (B) SVZ whole mount preparations show ADAM10 (red) expression at the ventricular surface co-localizing with GFAP⁺ (blue) NSC apical membranes at the center (arrowhead) of pinwheels (demarcated by β-catenin in green). Dotted line outlines pinwheel. (C) Experimental timeline of ADAM10 deletion from Nestin⁺ NSCs *in vivo*. (D) Representative quantitative reverse transcription-polymerase chain reaction and quantification of *ADAM10* mRNA, from YFP-sorted WT and ADAM10$^{fl/fl}$ cells. *P = 0.0479. (E) Representative coronal SVZ sections immunostained for GFAP (red) and Sox2 (green) 5 days after the final TAM injection. Inserts show high magnification of arrows. (F) Quantification of GFAP⁺Sox2⁺ cells. *P = 0.0247 (left) and EGFR⁺Sox2⁺ cells/total DAPI⁺ cells (from 417 WT and 453 ADAM10$^{fl/fl}$ cells), *P = 0.0498 (right). (G) Representative immunostaining of transit-amplifying EGFR⁺ cells (red) in acutely dissociated SVZ tissue from wild-type and ADAM10$^{fl/fl}$ animals. (H) Representative immunostaining of DCX⁺ neuroblasts in acutely dissociated SVZ tissue from WT and ADAM10$^{fl/fl}$ animals. (I) Quantification of the percentage of DCX⁺/total DAPI⁺ cells (from 1339 WT and 1348 ADAM10$^{fl/fl}$ cells). WT *vs.* ADAM10$^{fl/fl}$ samples, *P = 0.0339. (J) Immunoblotting for cleaved caspase 3 (17 kDa) in WT and ADAM10$^{fl/fl}$ NSCs differentiated *in vitro* for 2 days. (K) Quantification of cleaved caspase western blots. P = 0.2622. Statistics were performed with Student's unpaired *t*-test. For G n = 4, all others n = 3. Error bars represent the mean ± SEM. ADAM10: A disintegrin and metalloproteinase 10; DAPI: 4′,6-diamidino-2-phenylindole; DCX: doublecortin; EGFR: epidermal growth factor receptor; GFAP: glial fibrillary acidic protein; GFP: green fluorescent protein; SVZ: subventricular zone; YFP: yellow fluorescent protein; WT: wild-type.

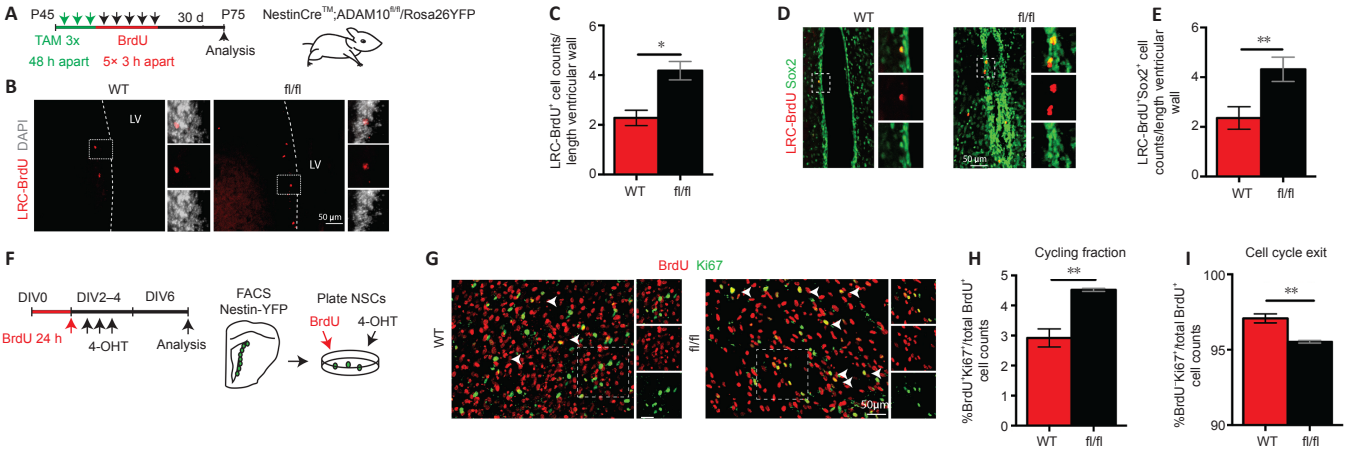

Figure 2 | **ADAM10$^{fl/fl}$ NSCs are retained in the cell cycle.**
(A) Experimental paradigm showing deletion of ADAM10 from Nestin⁺ NSCs and subsequent bromodeoxyuridine (BrdU) pulse-chasing *in vivo*. (B) Representative immunofluorescence of LRCs with persistent BrdU positivity 30 days after last BrdU injection in WT and ADAM10$^{fl/fl}$ mice. The dotted line demarcates the border of the lateral ventricle. (C) Quantification of data in B. In total, 148 and 301 LRC-BrdU⁺ cells were quantified. WT *vs.* ADAM10$^{fl/fl}$ cells, *P = 0.0136. (D) LRC-BrdU⁺ cells co-stained with the NSC marker Sox2 in the SVZ of WT and ADAM10$^{fl/fl}$ mice. The dotted box magnifies the area in the individual panels to the left, where each of the fluorophores is individually shown. (E) Quantification of data shown in D. 73 and 164 LTR-BrdU⁺Sox2⁺ cells were observed in the WT and ADAM10$^{fl/fl}$ SVZ. WT *vs.* ADAM10$^{fl/fl}$ cells, **P = 0.0053. (F) Experimental paradigm of BrdU labeling and ADAM10 deletion from cultured NSCs. Dissociated secondary neurospheres were plated on poly-L-lysine-treated coverslips. Cells were administered BrdU *in vitro* for 24 hours before the addition of 4-hydroxytamoxifen (4-OHT) and growth factor removal. (G) Co-staining for BrdU and Ki67 reveals the cycling cells (BrdU⁺Ki67⁺ cells; arrows) and those that have left the cell cycle (BrdU⁺Ki67⁻). Inserts show individual channels of the dashed white box. (H) Quantification of the percentage of BrdU⁺Ki67⁺/total BrdU⁺ cells shows more cycling cells in the ADAM10$^{fl/fl}$ cells. WT *vs.* ADAM10$^{fl/fl}$ cells, **P = 0.0064. (I) Quantification of the percentage of BrdU⁺Ki67⁻/total BrdU⁺ cells showing decreased cell cycle exit in the ADAM10$^{fl/fl}$ cells. 8662 and 9107 BrdU⁺ WT and ADAM10$^{fl/fl}$ cells were analyzed, respectively. WT *vs.* ADAM10$^{fl/fl}$ cells, **P = 0.0077. For A–D, n = 4 and E–F, n = 3 mice per group. At least five images per biologic replicate were analyzed. Student's unpaired *t*-test was used. Scale Bars: 50 μm. Error bars represent the mean ± SEM. ADAM10: A disintegrin and metalloproteinase 10; BrdU: bromodeoxyuridine; DIV: days *in vitro*; LRC: label-retaining cells; NSC: neural stem cell; WT: wild-type.

To further quantify the role of ADAM10 in the regulation of NSC cell cycle status under strictly-controlled temporal and environmental conditions, we studied NSCs in an *in vitro* culture system in which they form free-floating non-adherent spherical clusters of cells termed neurospheres (Reynolds and Weiss, 1992). After passaging, re-formation of neurospheres indicates retention of the self-renewal potential of stem cells, whereas differentiation to progenitors marks the loss of the ability for sphere formation. Secondary neurospheres are those that form following the first passage tertiary neurospheres following the second passage, and so forth. Deletion of ADAM10 in FAC-sorted YFP⁺ cells resulted in increased self-renewal, as measured by increased secondary (1.99 ± 0.32 over controls, P = 0.0253) and tertiary neurosphere formation (1.54 ± 0.20 over controls, P = 0.0092; **Figure 3A** and **B**). This result suggests a preference towards NSC identities retention over lineage progression. Furthermore, the ADAM10$^{fl/fl}$ neurospheres had a smaller diameter (57.81 ± 5.09 *vs.* 36.20 ± 2.67 μm in WT *vs.* ADAM10$^{fl/fl}$ YFP-sorted cells, respectively, P = 0.0001; **Figure 3D**) consistent with the decreased generation of rapidly dividing ADAM10$^{fl/fl}$ progenitors. The majority of ADAM10$^{fl/fl}$ neurospheres were less than 30 μm in diameter,

while WT neurospheres were 50 µm or greater, consistent with the decreased generation of rapidly dividing ADAM10$^{fl/fl}$ progenitors. The decrease in rapidly dividing cells was further confirmed after short term (2 hours) BrdU administration *in vitro* by analyzing the percentage of YFP$^+$BrdU$^+$ cells (35.83 ± 1.79% *vs*. 7.15 ± 6.77% YFP$^+$BrdU$^+$ cells/total YFP$^+$ cells in 427 WT and 727 ADAM10$^{fl/fl}$ cells, respectively, P = 0.0134). Similarly, as in the *in vivo* analysis, dissociated cultures of ADAM10$^{fl/fl}$ secondary neurospheres in differentiating conditions (7 days *in vitro*; DIV) produced reduced numbers of neurons (MAP2$^+$ cells; 0.51 ± 0.08 of controls, P = 0.00239) and retained higher numbers of undifferentiated cells (Nestin$^+$ cells 2.17 ± 0.48 of controls, P = 0.043; **Figure 3A–J**). These data suggest that ADAM10 is required for rapid cycling of NSCs and lineage progression to the neuronal phenotype.

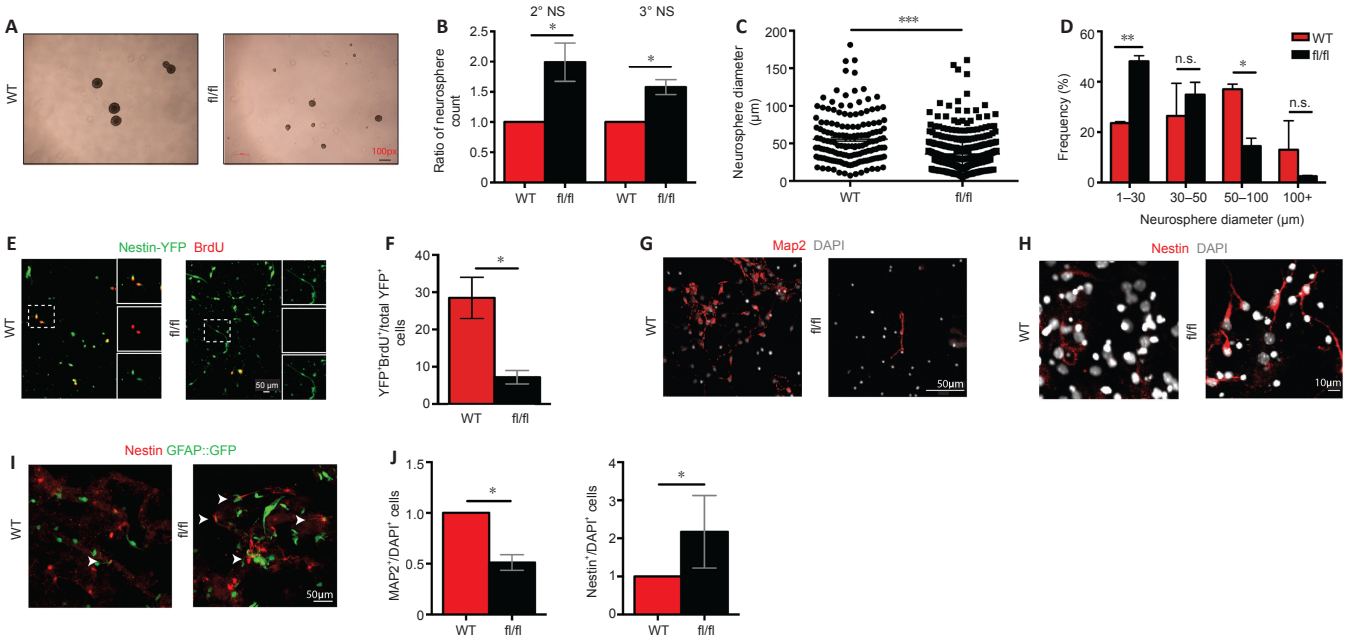

Figure 3 | Immunohistochemical analysis of WT and ADAM10$^{fl/fl}$ cells after 7 days in differentiation conditions reveals decreased neurogenesis in ADAM10$^{fl/fl}$ cells.
(A) Representative images of WT and ADAM10$^{fl/fl}$ secondary neurospheres from YFP sorted cells. (B) Analysis of WT and ADAM10$^{fl/fl}$ YFP$^+$ sorted cells *in vitro* demonstrated an increased formation of neurospheres following secondary (*P = 0.0444) and tertiary (*P = 0.0306) passaging. 2° NS: 2° neurosphere (passage 1); 3° NS: 3° neurosphere (passage 2). (C) Analysis of sphere diameter demonstrated YFP$^+$ADAM10$^{fl/fl}$ sorted cells were smaller compared to WT spheres (WT *vs*. ADAM10$^{fl/fl}$ YFP sorted cells, ***P = 0.0001). (D) Bins of neurosphere size showed WT spheres with wider diameter while more of the ADAM10$^{fl/fl}$ spheres were 1–30 µm in size (WT *vs*. ADAM10$^{fl/fl}$ YFP sorted cells, **P = 0.004 and *P = 0.013 for 1–30 µm and 50–100 µm, respectively; P = 0.478 and 0.328 for 30–50 µm and 100$^+$ µm, respectively). (E) Representative images from Nestin-YFP (green) sorted cells treated with BrdU 2 hours before processing for YFP and BrdU. (F) Quantification in E showed a decrease in the percentage of YFP$^+$BrdU$^+$/total YFP$^+$ cells. In total, 427 WT and 727 ADAM10$^{fl/fl}$ YFP$^+$ cells were quantified. WT vs. ADAM10$^{fl/fl}$ cell, *P = 0.0134. (G, H) Representative images of 2° NS-derived cells after *in vitro* differentiation stained for MAP2 (red) (G) and Nestin (red) (H). (I) Representative images of WT and ADAM10$^{fl/fl}$ NSCs from GFAP::GFP mice differentiated *in vitro*. Stained for Nestin (red) similarly demonstrate increased GFAP::GFP$^+$ cells (green) co-expressing the NSC marker Nestin (arrowheads). (J) Quantification of YFP sorted cell differentiation shows the percentage of MAP2$^+$ (left) cells and Nestin$^+$ cells (right) normalized over DAPI. The numbers are expressed as a ratio. 5804 and 5475 WT and ADAM10$^{fl/fl}$ cells were counted, respectively (MAP2$^+$ cells: 0.51 ± 0.08 of controls, *P = 0.0239; Nestin$^+$ cells: 2.17 ± 0.48 of controls, *P = 0.043). Scale bars: 50 µm in E, G, I, 10 µm in H. n = 3. Statistical analysis with Student's unpaired t-test. Error bars represent the mean ± SEM. ADAM10: A disintegrin and metalloproteinase 10; BrdU: bromodeoxyuridine; GFAP: glial fibrillary acidic protein; MAP2: microtubule-associated protein 2; NSC: neural stem cell; WT: wild-type; YFP: yellow fluorescent protein.

ADAM10 directs the positioning of NSCs within the basal and apical SVZ niche

Considering the defective differentiation of NSCs, we investigated whether deletion of ADAM10 in adult NSCs would have an effect on NSC positioning within the apical or basal SVZ. We used whole-mount preparations and confocal microscopy analysis. Five days following TAM administration, a different morphology was observed in the ADAM10$^{fl/fl}$ GFAP$^+$ NSCs, as a higher number of these cells extended long basal processes reminiscent of a "radial glia-like" morphology. All images were acquired using the same dynamic modifiers so as not to miss cell extensions. Also, at this time point, the number of GFAP$^+$ cells making direct contact with the blood vessels, visualized with laminin co-staining, was markedly decreased in ADAM10$^{fl/fl}$ NSCs (**Figure 4A** and **B**). To further characterize the positioning of NSCs *in situ*, GFAP-GFP$^+$ NSCs were analyzed in the Nestin-CRE^{ER}/ADAM10$^{fl/fl}$::GFAP-GFP mice which allowed for better visualization of the cell body of GFAP$^+$ NSCs and aided in quantification. The NSC positioning was analyzed by measuring the distance between the center of the NSC cell body to the nearest blood vessel, visualized by laminin staining, as well as the distance from the ventricular wall. In coronal SVZ sections, the ADAM10$^{fl/fl}$ GFAP-GFP$^+$ NSCs were closer to the ventricular wall (apical niche; 12.22 ± 0.68 µm *vs*. 21.1 ± 1.3 µm in WT) and farther from the blood vessel network (basal niche; 24.98 ± 1.38 µm *vs*. 16.08 ± 0.88 µm; P < 0.05, **Figure 4C** and **D**). ADAM10$^{fl/fl}$ NSCs were distributed closer to the ventricular wall, with the majority of ADAM10$^{fl/fl}$ NSCs found within 5 µm of the ventricular wall, while WT NSCs demonstrated an even distribution (**Figure 4E**). This result suggests that ADAM10 may regulate NSC positioning with respect to the apical and basal niches.

We then examined whether these observed effects of ADAM10 on NSC positioning and morphology were cell-autonomous or rather governed by the microenvironment in which these NSCs reside. Since ADAM10 can signal via autocrine, paracrine, or juxtacrine pathways (Schneider et al., 2012), these positioning and morphological phenotypes could be either cell-autonomous or non-autonomous processes. To this end, FAC-sorted Nestin-YFP$^+$ NSCs from WT and ADAM10$^{fl/fl}$ mice were seeded over WT SVZ explants, which provided a WT niche (**Figure 4F**). After 3DIV WT Nestin-YFP$^+$ cells displayed a rounded morphology with few processes (resembling NPCs), while ADAM10$^{fl/fl}$ YFP$^+$ cells displayed a radial glia-like morphology, and virtually no cells with NPC morphology were observed in the explants (**Figure 4G–J**), consistent with the observed morphology in the ADAM10$^{fl/fl}$ NSCs *in situ* wholemount preparations (**Figure 4A** and **B**). To determine whether this morphological phenotypic shift would be reflected in a change in cell fate, Nestin-YFP$^+$ cells were analyzed after seeding for stem and progenitor cell markers. A higher percentage of YFP$^+$ cells co-expressing the stem cell markers CD133 and Nestin were observed in the ADAM10$^{fl/fl}$ NSCs, suggesting that WT NSCs had undergone lineage progression from NSCs to NPCs. More ADAM10$^{fl/fl}$ cells were YFP$^+$CD133$^+$ or YFP$^+$Nestin$^+$ *vs*. WT cells (**Figure 4H–L**). Furthermore, there was no significant difference in the distance of YFP$^+$ cells from blood vessels in the two genotypes, indicating that ADAM10$^{fl/fl}$ NSCs can respond to endothelial-derived cues similarly to WT NSCs (**Figure 4M**). Together, these data suggest that deletion of ADAM10 preserves the apical niche in a quiescent state in a cell-autonomous fashion.

ADAM10 regulates the activation of junctional adhesion molecule C

To probe a mechanism by which ADAM10 regulates NSC positioning within the SVZ niche, we screened for global changes in gene expression in the ADAM10 knockout. Interestingly, microarray analysis of SVZ tissue 48 hours after TAM injections revealed reduced levels of several canonical ADAM10 substrates (potentially as a feedback loop in response to the elimination of ADAM10), including Eph receptors, ephrins, and JAMC. Here, we focused on JAMC as a potential molecular substrate for ADAM10 in NSCs, due to its identification as an apical surface marker of NSCs during cortical development, and as a substrate for ADAM10 cleavage in two endothelial cell lines, lung microvascular cells and human mammary epithelial cells (Rabquer et al., 2010; Stelzer et al., 2012). Immunostaining of coronal SVZ sections and whole mounts demonstrated that JAMC was highly expressed in the apical SVZ, but not the basal side of the ventricular wall indicating specific expression within the neurogenic niche. JAMC was also distinctively present at the center of the pinwheel structures, similar to ADAM10 localization,

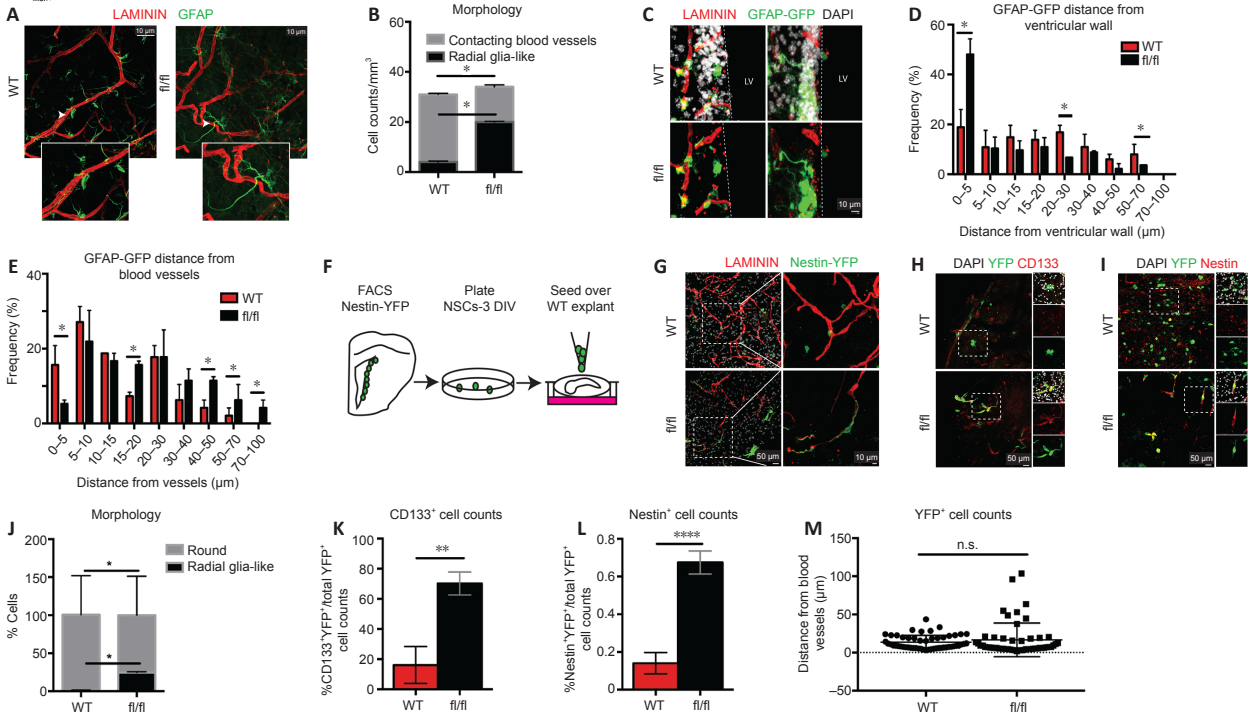

Figure 4 | **ADAM10 deletion promotes stemness and altered morphology in a cell-autonomous manner.**
(A) Representative whole-mount staining (5 days after the final tamoxifen injection) for GFAP (green) and laminin (red, staining for blood vessels) show normal pinwheel architecture in the apical niche. Arrows point to the areas that are magnified in the accompanying panels. (B) Quantification of basal niche including radial glia-like cells around the blood vessels in WT and ADAM10$^{fl/fl}$ SVZ, *$P \leq 0.05$. (C) Whole-mount SVZ preparations stained for GFAP (green) and laminin (red) in WT and ADAM10$^{fl/fl}$ mice in the basal SVZ niche. The dotted line demarcates the border of the ventricle. (D) Quantification showing the distribution frequency of GFAP$^-$GFP$^+$ NSCs from the ventricular wall. *Indicates $P < 0.05$ between adjacent columns as demarcated by the dashed line in C. (E) Quantification showing the distribution frequency of GFAP$^-$GFP$^+$ NSCs from the blood vessels. (F) Experimental paradigm showing FAC sorted Nestin$^-$YFP$^+$ cells from WT and ADAM10$^{fl/fl}$ mice grown *in vitro* before plating on WT SVZ slice cultures for 3 days followed by IF processing. (G) Coronal and GFAP::GFP SVZ sections immunostained for laminin (red) showing Nestin$^-$YFP$^+$ (green) ADAM10$^{fl/fl}$ NSCs in relationship to the ventricular wall and blood vessels. 704 and 274 WT and ADAM10$^{fl/fl}$ YFP$^+$ cells were analyzed for morphology, respectively. Inserts show high magnification of the dotted white box. (H) Representative image of an SVZ slice culture immunostained for YFP (green) and the NSC marker CD133 (red). High magnification insert of dotted white box (representative of the round morphology in WT *vs.* radial glia-like morphology in the fl/fl). In total, 52 and 91 WT and ADAM10$^{fl/fl}$ YFP cells were analyzed for co-expression with CD133. (I) Representative slice culture of YFP (green) and Nestin (red) co-expression. High magnification inserts of dotted white box shown to the right. In total, 330 and 135 WT and ADAM10$^{fl/fl}$ YFP$^+$ cells were analyzed for co-expression with Nestin, respectively. (J) Quantification of morphology in WT and ADAM10$^{fl/fl}$ YFP$^+$ cells, *$P < 0.05$. (K) Quantification of the percentage of CD133$^+$YFP$^+$/total YFP$^+$ cells. WT *vs.* ADAM10$^{fl/fl}$ cells, **$P = 0.0048$. (L) Quantification of Nestin$^+$YFP$^+$/total YFP. WT *vs.* ADAM10$^{fl/fl}$ cells, ****$P = 0.0001$. (M) YFP$^+$ cell distance from blood vessels immunostained for laminin. WT *vs.* ADAM10$^{fl/fl}$ cells, $P = 0.3473$. For A–E, $n = 3$. For F–J, at least four explants were analyzed in two independent experiments for eight explants. Scale bars: 10 µm in A, C, G and 50 µm in H, I. Two-way analysis of variance with Tukey multiple comparisons in D and E, all others are unpaired *t*-test. Error bars represent the mean ± SEM. ADAM10: A disintegrin and metalloproteinase 10; GFAP: glial fibrillary acidic protein; GFP: green fluorescent protein; NSC: neural stem cell; SVZ: subventricular zone; WT: wild-type; YFP: yellow fluorescent protein.

where it co-localized to the apical surface of GFAP$^+$ Type B NSCs (arrowhead; **Figure 5A**). Co-localization analysis *in vivo* showed that JAMC was present near the ventricular surface and associated with GFAP$^+$ cells. JAMC presence was verified in NSCs *in vitro*, where JAMC localized on the membrane of Nestin$^+$ stem and progenitor cells in acutely dissociated SVZ tissue (**Figure 5B** and **C**). Moreover, immunoprecipitation experiments with JAMC suggested an interaction between ADAM10 and JAMC, suggesting that ADAM10 may act to shed JAMC in the SVZ (**Figure 5D**).

Given that NSCs express both JAMC and ADAM10, and that they interact in the SVZ, we sought to investigate whether ADAM10 sheds JAMC and leads to signal activation. We used SVZ explants which were treated with vehicle or acitretin, a vitamin A analog that has been previously shown to stimulate ADAM10 promoter activity with an EC50 of 1.5 µM and increase the mature ADAM10 protein (Tippmann et al., 2009; Holthoewer et al., 2012). Increased ADAM10 activity in SVZ extracts following acitretin administration was first verified using an ADAM10 activity assay, where ADAM10 cleaves a FRET substrate resulting in measurable fluorescence. In a proof of concept experiment, the cleavage of N-cadherin (C-terminal fragment) by acitretin in the SVZ served as a biologic readout of increased ADAM10 activity (Reiss et al., 2005; Klingener et al., 2014).

Western blot analysis using an antibody targeted to the N-terminal domain of JAMC identified a 42 kDa full-length protein in vehicle-treated SVZ explants. When samples were treated with acitretin to increase ADAM10 activity, a soluble 25 kDa fragment was also identified (**Figure 5E** and **F**) with a corresponding decrease in the full length (42 kDa) JAMC (**Figure 5E** and **F**), indicating a functional interaction between ADAM10 and JAMC. Generation of this cleavage product was attenuated in acitretin-treated ADAM10$^{fl/fl}$ samples, indicating JAMC cleavage is ADAM10-mediated (**Figure 5E** and **F**). Further, we observed an increase in full-length JAMC in the ADAM10$^{fl/fl}$ sample and the presence of the small molecule inhibitor of ADAM10 GI254023X compared to controls (1.77 ± 0.14 of controls, $P = 0.0431$; data not shown).

Next, we investigated whether JAMC cleavage impacts downstream signals to guide NSC behavior. We focused on RAP1, a member of the Ras family of small GTP binding proteins that can switch from an active GTP-bound form and an inactive GDP-bound one (Bos et al., 2003). Previous studies demonstrated decreased RAP1 activity following JAMC overexpression, while JAMC ablation increased RAP1 activity, highlighting RAP1 as a downstream target of JAMC signaling (Orlova et al., 2006; Li et al., 2009). RAP1-GTPase Activating Protein (RAP1Gap) acts as a negative regulator of active RAP1-GTP by promoting the conversion to the GDP-bound form (Bos et al., 2003). If ADAM10 activates JAMC signaling, then it is possible that increased ADAM10 activity would result in increased RAP1Gap. Cleavage of JAMC correlated with an increase in RAP1Gap levels in mice treated with acitretin, suggesting that RAP1Gap also acts downstream of ADAM10 (**Figure 5F–H**). Together, these findings are consistent with prior observations that RAP1 activity decreases following JAMC overexpression, while JAMC ablation increases Rap1 activity, highlighting RAP1 as a downstream target of JAMC signaling, and a potential effector (Orlova et al., 2006; Li et al., 2009).

We further verified the presence of RAP1GAP expression in NSCs undergoing *in vitro* differentiation as demonstrated by expression of the neuroblast fate marker DCX (**Figure 6A**). Rap1Gap was expressed at higher levels in cells from the ventricular wall, while very few cells adjacent to the wall expressed RAP1Gap, consistent with a role for RAP1Gap in apical-to-basal transit (**Figure 6B** and **C**). These findings are in line with cortical embryonic (E18.5) and postnatal SVZ (P4) stages where RAP1-GTP is higher in NSCs, while RAP1Gap is higher in cells undergoing differentiation and emigrating from the niche following commitment towards a migratory neuroblast fate (Niola et al., 2012). We observed a similar pattern of expression of RAP1Gap, demonstrating preservation of this mechanism, in the adult SVZ. In support of the hypothesis that ADAM10 regulates JAMC/RAP1Gap signaling in NSCs, increased RAP1-GTP and a corresponding decrease in RAP1Gap were detected in ADAM10$^{fl/fl}$ NSCs (**Figure 6D** and **E**). This observation was further validated using the small molecule ADAM10 inhibitor, GI254023X (GI). Incubation of NSCs with GI showed a similar trend towards a decrease in RAP1Gap, and an increase in the full-length form of JAMC, as compared with vehicle (0.72 ± 0.09 of controls, $P = 0.0547$; data not shown).

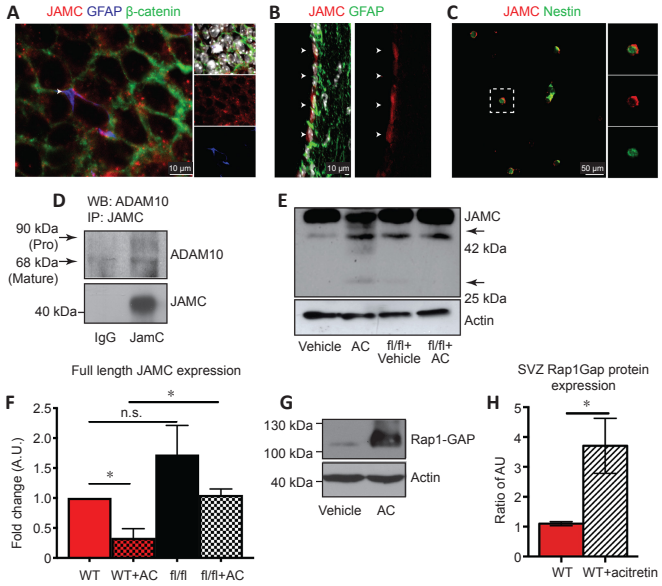

Figure 5 | JAMC is a feature of adult NSCs and is cleaved by ADAM10 in the WT SVZ.
(A) Whole-mount staining for JAMC$^+$ cells (red) and GFAP$^+$ cells (blue) at NSC contacts at the center (arrowhead) of pinwheels (green). Panel to right is a magnification of the arrowhead. (B) JAMC expression in GFAP$^+$ NSCs along the wall of the lateral ventricle (arrowheads). (C) JAMC expression in Nestin$^+$ stem cells in acutely dissociated WT SVZ tissue. High magnification inserts of the dashed white box. (D) Immunoprecipitation of JAMC and ADAM10 in SVZ tissue lysates. The 90 kDa pro-form and 68 kDa mature form of ADAM10 are indicated. (E) Immunoblot of SVZ slice cultures from WT and ADAM10$^{fl/fl}$ mice treated with hydroxytamoxifen *in vitro* and acitretin (AC) probed for JAMC. A JAMC fragment (25 kDa) is shown by an arrow in WT AC-treated samples. (F) Quantification of full length JAMC protein expression in WT, WT + acitretrin, ADAM10$^{fl/fl}$, and ADAM10$^{fl/fl}$ + acitretin treated groups (WT + acitretin *vs.* ADAM10$^{fl/fl}$ + acitretin, $^*P = 0.0174$; WT *vs.* WT + acitretin, $^*P = 0.0123$; WT + acitretin *vs.* ADAM10$^{fl/fl}$, $P = 0.2903$). (G) Immunoblotting of SVZ tissue in WT- and AC-treated mice for RAP1Gap. (H) Quantification of RAP1Gap protein levels in WT and WT + acitretin treated groups. $^*P = 0.0203$. For A–C, representative images are shown, $n = 3$; D–F, $n = 3$; G, $n = 12$. Scale Bars: 10 μm in A, B and 50 μm in C. For all, Students' unpaired *t*-test was used. Error bars represent the mean ± SEM. AC: Acitretin; ADAM10: A disintegrin and metalloproteinase 10; GFAP: glial fibrillary acidic protein; JAMC: junctional adhesion molecule C; NSC: neural stem cell; SVZ: subventricular zone; WT: wild-type.

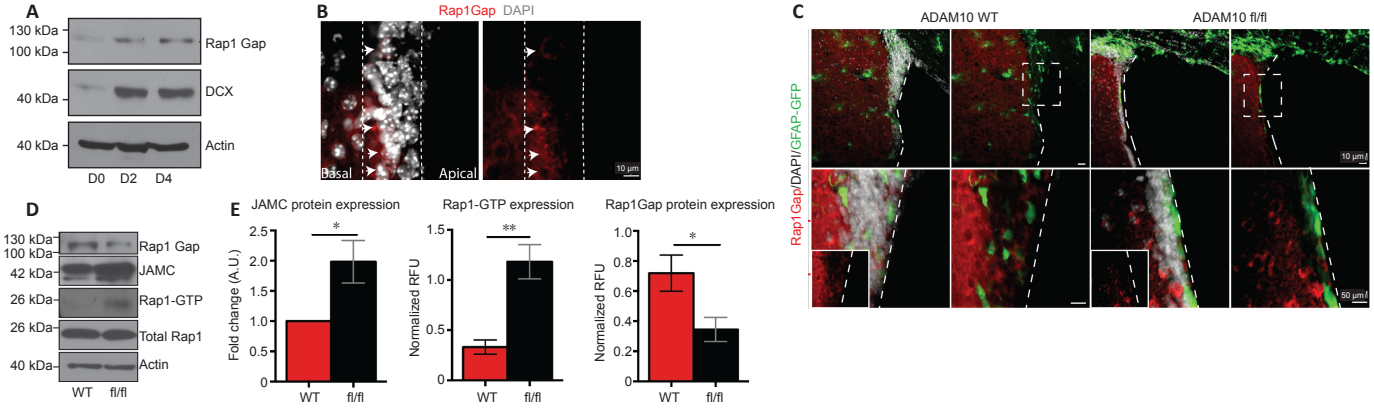

Figure 6 | RAP1Gap is expressed in progenitors in the basal adult SVZ niche.
(A) Representative immunoblot of RAP1Gap protein levels in WT NSCs in differentiating conditions for the indicated days (D) D0 to D4. (B) Representative sagittal SVZ section showing RAP1Gap expression (red) in regions around the ventricular wall (dotted line), apical and basal niche on the striatal side of the SVZ. Arrowheads point to high expression of RAP1Gap. (C) Expression of Rap1Gap in the GFAP-GFP$^+$ NSCs in coronal SVZ sections in WT and ADAM10$^{fl/fl}$ brains. The dashed box in the top panel with high magnification insert in the bottom panel. The dashed line represents the ventricular wall. (D) Immunoblot analysis for JAMC, RAP1-GTP (active RAP1), RAP1Gap, and total RAP1 protein levels in WT and ADAM10$^{fl/fl}$ cells. (E) Quantification of full length JAMC, RAP1-GTP, RAP1Gap protein expression in WT and ADAM10$^{fl/fl}$ NSCs, $^*P = 0.0496$, $^{**}P = 0.0017$, $^*P = 0.0322$, respectively. For A–C, $n = 3$; D, E, $n = 5$. Scale bars: 10 μm in B and C (upper) and 50 μm in C (lower). Student's unpaired *t*-test was performed. Error bars represent the mean ± SEM. ADAM10: A disintegrin and metalloproteinase 10; GFAP: glial fibrillary acidic protein; GFP: green fluorescent protein; JAMC: junctional adhesion molecule C; NSC: neural stem cell; SVZ: subventricular zone; WT: wild-type.

Moreover, differentiation of ADAM10$^{fl/fl}$ cells did not result in the same increase in RAP1Gap seen in WT NSCs. Not only were levels lower than WT in proliferating ADAM10$^{fl/fl}$ cells, but also no significant difference was observed between ADAM10$^{fl/fl}$ cells at day 0 (D0) or after 4 days in differentiating conditions (D4) *in vitro*. In WT NSCs, RAP1Gap expression increased significantly after 4 days (D4) in differentiating conditions, whereas ADAM10$^{fl/fl}$ NSCs demonstrated no such change (**Figure 7A–C**). Interestingly, a correlation was observed between JAMC and RAP1Gap during lineage progression. JAMC expression increased from D0 to D4 of differentiation (**Figure 7A**). This observation is in line with a previous study implicating JAMC recruitment to the cell surface in the adhesion-dependent exit of neuronal progenitors from their germinal zone (Famulski et al., 2010).

To determine whether JAMC overexpression could rescue RAP1Gap levels in ADAM10$^{fl/fl}$ NSCs, which would further support a critical role of JAMC in the regulation of RAP1Gap, we transfected NSCs with control or a pJAMC expression vector. Cell lysates were processed after 48 hours. JAMC overexpression rescued ADAM10 signaling in ADAM10$^{fl/fl}$ NSCs to WT levels, as increased RAP1Gap was detected in a pattern similar to that of WT NSCs (**Figure 7D** and **E**). These results are consistent with JAMC's known function of coordinating intracellular signaling and cell-cell contacts through recruitment of RAP1Gap (Orlova et al., 2006; Li et al., 2009).

To define whether RAP1Gap acts downstream of JAMC in NSCs, lentivirus was used to deliver shRNA targeted against JAMC *in vitro* (**Figure 7F** and **G**). Similar to the ADAM10$^{fl/fl}$ NSCs, a decrease in RAP1Gap expression was observed after JAMC knockdown in WT NSCs (**Figure 7F** and **G**), demonstrating that the decrease in RAP1Gap observed in the ADAM10$^{fl/fl}$ NSCs was due to decreased signaling in a pathway that includes JAMC. These results implicate RAP1Gap as a downstream effector of both ADAM10 and JAMC.

To place RAP1Gap downstream of ADAM10 and determine the effect of ADAM10 deletion on differentiation, we overexpressed RAP1Gap *in vitro* using a lentiviral approach. As an initial validation, we verified that lentiviral overexpression of RAP1Gap indeed rescued RAP1-GTP expression in ADAM10$^{fl/fl}$ NSCs to WT levels. To investigate the effect of overexpression on lineage progression, control and RAP1Gap lentivirus transduced ADAM10$^{fl/fl}$ NSCs were plated on top of WT SVZ explants, and then co-expression analysis with NSC and progenitor markers was performed (**Figure 7H**). Co-expression analysis revealed a decrease in RAP1Gap infected ADAM10$^{fl/fl}$ NSCs co-expressing CD133 (prominin) compared to control infected ADAM10$^{fl/fl}$ NSCs (GFP$^+$CD133$^+$ cells/total GFP$^+$ cells; **Figure 7I** and **J**). However, no significant changes were observed in Nestin$^+$GFP$^+$ cells between groups (GFP$^+$Nestin$^+$ cells/total GFP$^+$ cells; **Figure 7I** and **J**). Together, these results suggest that RAP1Gap acts downstream of ADAM10 to mediate effects on cell cycle progression.

We also observed an increase in VCAM1 expression in ADAM10$^{fl/fl}$ cell lysates (**Figure 7K** and **L**) and in wholemount stained sections (data not shown), which served as a phenotypic readout of increased adhesion to the ventricular wall and correlated with the data that demonstrated higher NSC adhesion within the apical niche (**Figure 4**). This increased VCAM1 expression recovered to WT levels by the increase in RAP1Gap following JAMC overexpression in the ADAM10$^{fl/fl}$ samples and was consistent with decreased ADAM10 activity promoting an undifferentiated NSC state of downstream of JAMC. Taken together, these results suggest that ADAM10 may regulate JAMC shedding in NSCs resulting in increased RAP1Gap and a concurrent decrease in active RAP1. Via this mechanism, ADAM10 could regulate the balance between niche adhesion and promote lineage progression.

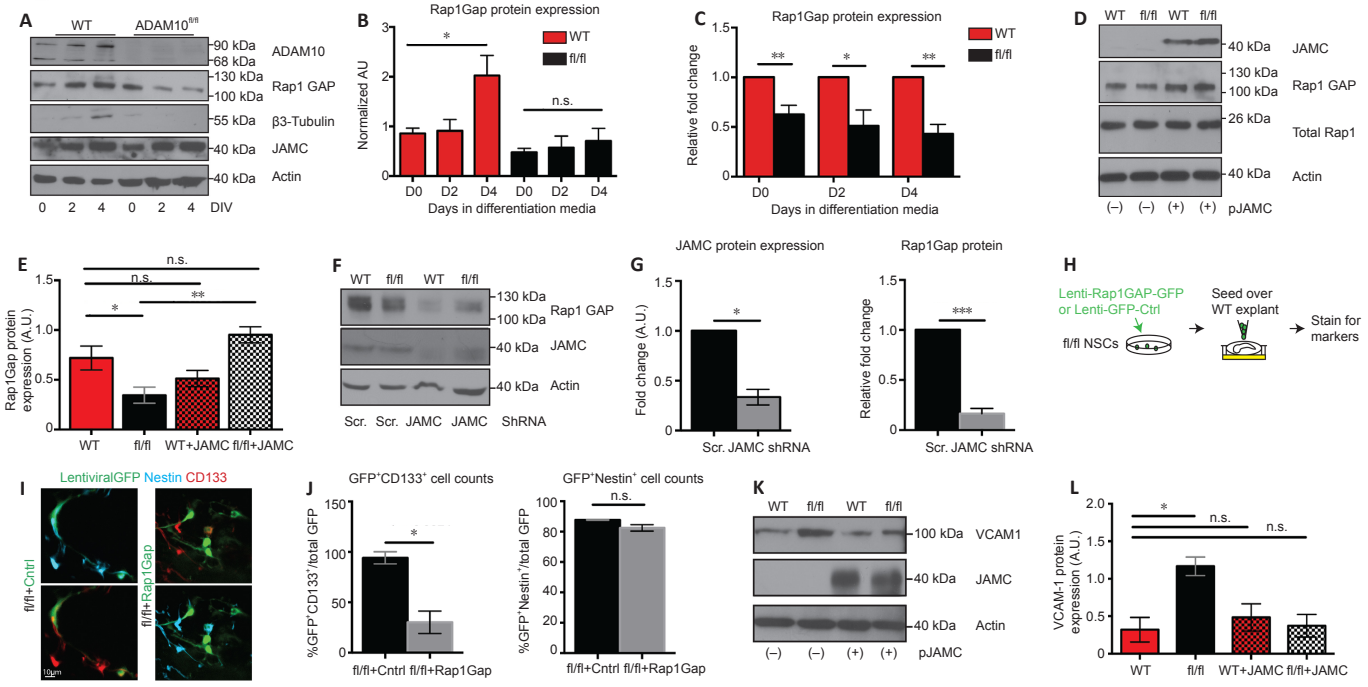

Figure 7 | **RAP1Gap acts downstream of ADAM10 and JAMC.**

(A) Representative immunoblots of RAP1Gap and JAMC protein expression during *in vitro* differentiation in WT and ADAM10$^{fl/fl}$ cells. (B) Quantification of the data from A at 0, 2, and 4 days *in vitro* (DIV). WT: 0.86 ± 0.11 on day 0 (D0) under differentiation conditions to 2.02 ± 0.41 on day 4 differentiation conditions (D4) (*P = 0.0448). ADAM10$^{fl/fl}$: from 0.48 ± 0.08 on D0 to 0.71 ± 0.26 on D4 (P = 0.4874). (C) Fold change in RAP1Gap expression in ADAM10$^{fl/fl}$ cells during differentiation at 0, 2, and 4 DIV in comparison to WT (**P = 0.0062, *P = 0.0458, **P = 0.0267); V: ventricle. (D) Representative immunoblot of RAP1Gap expression in ADAM10$^{fl/fl}$ cells recovered to WT levels after JAMC overexpression. (E) Quantification of the data in D. WT *vs.* ADAM10$^{fl/fl}$, *P = 0.0322; ADAM10$^{fl/fl}$ *vs.* ADAM10$^{fl/fl}$ + JAMC, **P = 0.0026. (F) Representative western blot of RAP1Gap expression showing a decrease after lentivirally delivered shRNA targeted to JAMC in WT cells with JAMC knockdown and RAP1Gap. (G) Quantification of the data from F. After infection, the shRNA decreased JAMC expression to 0.33 ± 0.08 of controls, *P = 0.0137. After infection, the shRNA decreased Rap1Gap expression to 0.16 ± 0.05 of controls, ***P = 0.0001. (H) Rap1GAP-GFP lentivirally-transduced cells were plated on WT SVZ explants *in vitro* before processing for CD133 and Nestin co-expression. High expression of Rap1GAP-GFP was assessed by immunoblot assay (Figure 8G). (I) Representative images of Nestin and CD133 staining in ADAM10-deleted cells treated with control (Ctr) lentivirus or lenti-Rap1Gap overexpression vector. Scale Bar: 10 μm. (J) Quantification of the data from I showing a decrease in CD133 expression in RAP1Gap overexpressing cells and no significant change in GFP co-expression with Nestin. 43 ADAM10$^{fl/fl}$ GFP$^+$ cells and 71 ADAM10$^{fl/fl}$ + RAP1Gap GFP$^+$ cells were quantified in total. 93.98 ± 6.02% of ADAM10$^{fl/fl}$ GFP$^+$ control cells *vs.* 30.21 ± 11.17% of ADAM10$^{fl/fl}$ GFP$^+$ cells over-expressing RAP1Gap co-expressed with CD133, *P = 0.0374. 87.83 ± 0.33% *vs.* 82.5 ± 2.1% of control and RAP1Gap ADAM10$^{fl/fl}$ GFP$^+$ cells co-expressed with Nestin, respectively, P = 0.1292. (K) Representative immunoblots of VCAM-1 protein expression in WT, ADAM10$^{fl/fl}$, and JAMC overexpressing cells. (L) Quantification of the data in K (*P = 0.0148). n = 3 unless otherwise indicated. Analysis of variance with Tukey's multiple comparisons was used in E and L, Student's unpaired t-test for all others. Error bars represent the mean ± SEM. ADAM: A disintegrin and metalloproteinase 10; GFP: green fluorescent protein; JAMC: junctional adhesion molecule C; WT: wild-type.

Transit and positioning of NSCs into the apical and basal niche is regulated by ADAM10 via JAMC/RAP1Gap

Our data suggest that ADAM10 regulates NSC positioning within the niche via JAMC/RAP1Gap, but are there functional consequences of this molecular interaction *in vivo*? To explore potential functional implications, we examined adhesive and transitory properties of WT and ADAM10$^{fl/fl}$ NSCs, as suggested by the abnormal NSC positioning in ADAM10-deleted NSCs (**Figure 4**), using *in vitro* scratch/wound assays as a surrogate for NSC adhesion and transit (Liang et al., 2007; Krishnaswamy and Korrapati, 2014; Graziola et al., 2017). Neurospheres were grown under identical culture conditions as those used in the experiments in **Figure 6**. When cells reached 80–90% confluence, a pipette tip was used to create a scratch in the monolayer, and distances of individual cells from the scratch edge were analyzed 24 hours later. ADAM10$^{fl/fl}$ NSCs were found at significantly shorter distances from the edge as compared with WT NSCs (**Figure 8A** and **B**). To further verify that this impaired phenotype was typical of ADAM10$^{fl/fl}$ NSCs, the scratch/wound assays were performed using GFAP-GFP$^+$ cells. Analyzing only GFAP-GFP$^+$ cells, ADAM10$^{fl/fl}$ cells were found at significantly shorter distances from the scratch edge compared with WT cells (**Figure 8C** and **D**).

As both ADAM10$^{fl/fl}$ and JAMC knockdown produced a decrease in RAP1Gap, the question arose whether a similar decrease in transitory potential as seen in the ADAM10$^{fl/fl}$ cells would be observed in the JAMC knockdown condition. The same scratch test was performed in WT and ADAM10$^{fl/fl}$ monolayers treated with the lentiviral vector expressing either scrambled (Scr) or JAMC shRNA. The decrease observed between WT + Scr and WT + shRNA NSCs was comparable to that under the ADAM10$^{fl/fl}$ condition (**Figures 7F**, **8E**, and **8F**) when analyzing the distance from the scratch edge. Increased RAP1Gap expression was observed when Rap1Gap was delivered via lentivirus to NSCs, yet the increase in ADAM10$^{fl/fl}$ NSCs was lower than the WT NSCs (**Figure 8G**). These results imply that the decreased translocation potential of ADAM10$^{fl/fl}$ NSCs is due to a decrease in the ADAM10-JAMC-RAP1Gap-RAP1 pathway.

To test whether NSCs lacking ADAM10 stick more to the apical surface of the SVZ, we assessed adhesion to different ECM components using short-term adhesion assays. Using a Calcein AM-based test, WT and ADAM10$^{fl/fl}$ NSCs were allowed to adhere to laminin, PLL, and fibronectin substrates in the presence of JAMC blocking antibody or isotype control IgG to investigate whether JAMC acts downstream of ADAM10-mediated NSC adhesion. Increased adhesion of ADAM10$^{fl/fl}$ NSCs to laminin only was observed, and this increase was rescued to WT levels after incubation with JAMC blocking antibody, indicating that the increased adhesion in ADAM10$^{fl/fl}$ cells is JAMC-dependent (**Figure 9A**). In further support, the adhesion experiments were repeated in the presence of GI 254023X, the small molecule inhibitor of ADAM10, as well as the small molecule Rap1 activator 8-CPT-2-O-Me-cAMP (Bryn et al., 2006). As above, inhibition of ADAM10 activity with GI 254023X increased adhesion of WT treated cells to a laminin substrate, while treatment with the Rap1 activator showed a trend towards an increase in adhesion when plated on laminin (**Figure 9B**). These results demonstrate that inhibition of ADAM10 activity promotes increased NSC adhesion to a laminin substrate and correlates the increase in RAP1 levels to the increase in adhesion (Kokovay et al., 2010).

ADAM10 supports the production of neurons in the olfactory bulb and short-term olfactory memory

Having dissected the molecular interactions downstream of ADAM10 regulating NSC cycling and positioning in the SVZ, we sought to determine whether ADAM10 deletion would lead to any functional sequelae *in vivo*. We investigated the cellular and functional outcomes of neurogenesis into the olfactory bulb (OB) and olfactory discrimination memory, which depends on these adult-born neurons (Breton-Provencher et al., 2009; Moreno et al., 2009; Kageyama et al., 2012; Wang et al., 2015). Mice were injected with TAM (as above) and analyzed 30 days later to allow time for Nestin$^+$ cells to migrate from their origin in the SVZ, through the rostral migratory stream (RMS), to their final destination in the granule cell layer of the OB. At this time point, the number of YFP$^+$ cells *en route*, both entering the RMS and within the granule cell layer, was significantly reduced (53.56 ± 1.74 cells/mm^3 *vs.* 24.98 ± 2.09 cells/mm^3, P = 0.001) in the ADAM10$^{fl/fl}$ mice (**Figure 10A–D**). Co-immunostaining with NeuN was performed to further confirm neuronal identity and maturation of YFP$^+$ cells in the granule cell layer. Although the density of mature neurons (YFP$^+$NeuN$^+$ cells) in the ADAM10$^{fl/fl}$ mice was significantly reduced, the percentage of newly generated neurons within the YFP population (YFP$^+$NeuN$^+$ cells/total YFP$^+$ cells) was unchanged (**Figure 10C** and **D**), indicating that the maturation program of neuroblasts in the ADAM10$^{fl/fl}$ mice was not affected. This most likely arises due to the timing of ADAM10 deletion in NSCs *versus* neuroblasts and suggests that once NPCs are able to leave the niche, their differentiation program is unaffected.

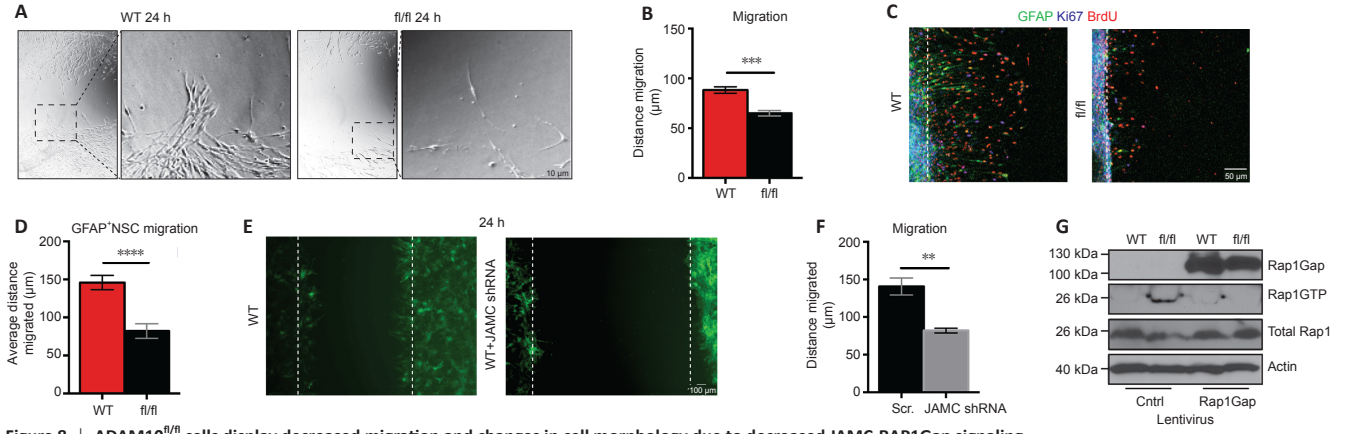

Figure 8 | ADAM10$^{fl/fl}$ cells display decreased migration and changes in cell morphology due to decreased JAMC-RAP1Gap signaling.
(A) Representative images of scratch test migration assays from monolayers of WT and ADAM10$^{fl/fl}$ NSCs. Distance of individual cell migration from the edge was analyzed at 24 hours using the ImageJ64 line measure tool. (B) Quantification of the data in A. 551 WT cells and 304 cells from three wells performed in triplicate (biologic replicates) were analyzed. On average, WT NSCs were 104.7 ± 2.76 µm while ADAM10$^{fl/fl}$ NSCs were 63.45 ± 1.65 µm from the scratch edge, ***P = 0.0001. (C) Representative immunofluorescence of GFAP::GFP (green) cell migration at 24 hours after plating on PLL coated coverslips. Migratory cells co-express with proliferation markers Ki67 (purple) and BrdU (red). (D) Quantification of the data in C from 100 WT GFAP-GFP$^+$ cells and 50 ADAM10$^{fl/fl}$ GFAP-GFP$^+$ cells from three coverslips repeated in triplicate. On average WT GFP$^+$ cells were 145.80 ± 9.42 µm while ADAM10$^{fl/fl}$ GFP$^+$ were 82.13 ± 9.58 µm from the edge, ****P = 0.0001. (E) Scratch test migration assays were performed in monolayer cells treated with scrambled or JAMC lentivirus-shRNA. (F) Quantification of the data shown in E. On average, control cells were found 118.12 ± 5.26 µm and shRNA treated cells were found 87.71 ± 4.72 µm, **P = 0.0076. (G) Representative immunoblots depicting the effect of lentivirally delivered RAP1Gap on RAP1-GTP in WT and ADAM10$^{fl/fl}$ NSC. For G n = 2, A–F n = 3. For slice cultures at least four explants were analyzed. For all, Student's unpaired t-test was used. Error bars represent the mean ± SEM. ADAM10: A disintegrin and metalloproteinase 10; BrdU: bromodeoxyuridine; GFAP: glial fibrillary acidic protein; GFP: green fluorescent protein; JAMC: junctional adhesion molecule C; WT: wild-type.

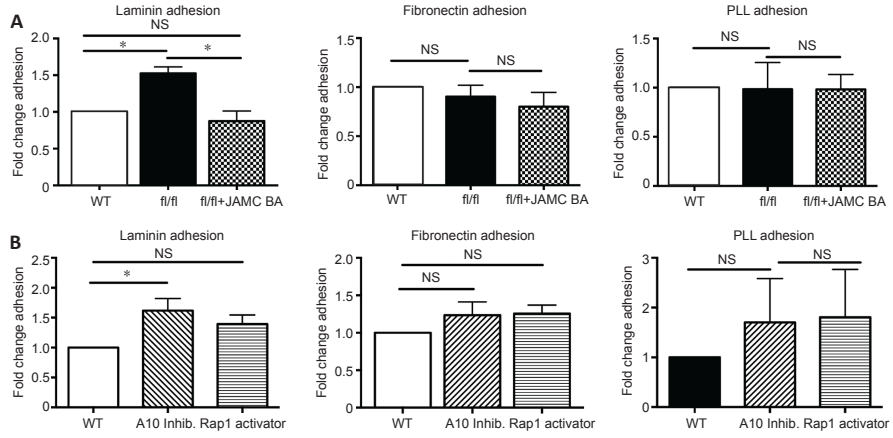

Figure 9 | JAMC and RAP1 direct NSC adhesion.
(A) Calcein-stained WT and ADAM10$^{fl/fl}$ NSCs were plated in the presence of JAMC blocking antibody or isotype control IgG and allowed to adhere to laminin, fibronectin, or poly-L-lysine (PLL) substrate. After a 20-minute incubation, non-adherent cells were gently washed away and the remaining fluorescence was calculated as a percentage of total fluorescence before washing, representing adhesion of ADAM10$^{fl/fl}$ NSCs to substrates (adhesion to laminin was significant at 1.53 ± 0.09 of controls, *P = 0.0037). This decreased by 0.63 ± 0.003 (*P = 0.001). (B) WT NSCs were treated with vehicle or the ADAM10 small molecule inhibitor GI254023X or the small molecule RAP1 activator 8-CPT-2-O-Me-cAMP and then cell adhesion to laminin, fibronectin, and poly-L-lysine was assessed. n = 3 in triplicate. A10 inhibitor: 1.62 ± 0.20 of controls, *P = 0.0380; Rap1 activator: 1.39 ± 0.15 of controls, P = 0.0598. One-way ANOVA with analysis of variance multiple comparisons. Error bars represent the mean ± SEM. ADAM10: A disintegrin and metalloproteinase 10; Inhib: inhibitor; JAMC: junctional adhesion molecule C; NSC: neural stem cell; WT: wild-type.

Adult neurogenesis is important for complex forms of olfactory behavior, such as short-term olfactory discrimination memory (Breton-Provencher et al., 2009; Moreno et al., 2009; Kageyama et al., 2012; Wang et al., 2015). Given the importance of ADAM10 in adult NSC cycling, migration, and neurogenesis as demonstrated above, we determined whether ADAM10 knockout from NSCs would lead to any behavioral consequences. To this end, we performed an olfactory memory task in ADAM10$^{fl/fl}$ mice treated with TAM to delete ADAM10 and control WT mice. The test of olfactory memory is based on the premise that mice generally spend more time exploring an odor they have not previously encountered, hence, when presented with the same odor at a short interval, mice will spend less time investigating a familiar odor (Breton-Provencher et al., 2009). WT and ADAM10$^{fl/fl}$ mice were assayed using the cotton tip-based test for short-term olfactory memory beginning 2 weeks after the final TAM injection (**Figure 10E**). No significant differences were observed in time spent investigating a control swab versus a presented odor between WT and ADAM10$^{fl/fl}$ animals, suggesting that preference for the odor was not affected. However, differences were observed in short-term olfactory memory, as a significant reduction in odor investigation was evident in the WT group at 30 minutes and 1 hour, however, this was not the case for ADAM10$^{fl/fl}$ mice at the same time points (**Figure 10E**). These observations point to a possible role of ADAM10 in adult neurogenesis-related short-term olfactory memory, although additional work will be required to confirm these findings using pharmacological, genetic, and behavioral studies.

Discussion

Retention of NSCs within the SVZ niche is critical for NSC maintenance. In particular, adhesion to the apical niche appears to modulate NSC quiescence (Shen et al., 2008). While the diverse array of cues that regulate SVZ residence through either NSC-NSC or NSC-niche interactions remain largely undefined, identification of molecules that mediate the balance between NSC maintenance and lineage progression will facilitate the development of cell replacement therapies. Our data show that the protease, ADAM10, maintains the pool of NSCs and their lineage cells by regulating adhesion to the apical SVZ domain upstream of a JAM-C/Rap1 axis.

During embryogenesis, ADAM10 deletion in NSPCs leads to progenitor depletion due to premature neuronal differentiation (Jorissen et al., 2010). In the adult, we observed a decrease in OB neurogenesis and an increase in NSC self-renewal after ADAM10 deletion which could be attributed to differences in the timing of deletion during embryogenesis versus adult period. While neurogenesis in the adult is restricted to the production of granule and periglomerular cells of the olfactory bulb, during embryogenesis the entire brain is populated by all stages of glial and neuronal lineages (Zhao et al., 2008; Ming and Song, 2011).

In vitro, we observed an increase in secondary neurosphere formation as well as retention of Nestin$^+$ cells under differentiation conditions, demonstrating that ADAM10 deletion promotes maintenance of NSC properties. Consistent with these findings, we observed an increase in slowly cycling BrdU label-retaining cells (LRC-BrdU) in the ADAM10$^{fl/fl}$ SVZ *in vivo* (Johansson et al., 1999a).

The phenotypic output was a decrease in newborn neurons reaching the OB, resulting in impaired short-term olfactory memory. In the OB, ongoing neurogenesis supplies interneurons necessary to maintain inhibitory strength within the OB network (Breton-Provencher et al., 2009; Arenkiel, 2010). We posit that the difference in neurogenesis measured in the OB is the result of impaired NSC lineage commitment. However, we previously showed that deletion of ADAM10 in NPCs delayed migration into the subcortical white matter (Klingener et al., 2014) and could not exclude that neuroblast migration is also affected. Future experiments studying aspects of olfactory behaviors, such as object discrimination and odor threshold, will determine the role of ADAM10 in olfaction.

Our data suggest that inhibition of ADAM10-initiated pathways maintains the undifferentiated state of NSCs in the adult SVZ, prompting an examination of positioning. Frequency analysis showed GFAP-GFP$^+$ NSCs in the ADAM10$^{fl/fl}$ mice distributed closer to the ventricular wall, while WT NSCs showed a more even distribution throughout the SVZ. This increased "stickiness" to the ventricular wall likely explains the increased NSC maintenance following ADAM10 deletion.

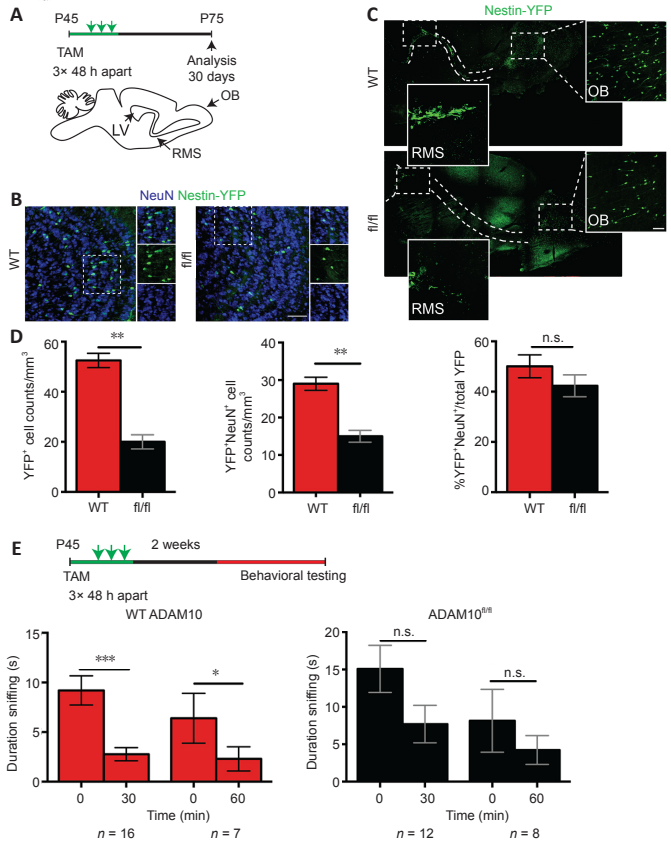

Figure 10 | ADAM10 deletion in the adult SVZ decreases olfactory neurogenesis in the granule cell layer of the OB *in vivo*.
(A) Top: Experimental timeline of ADAM deletion from NSCs and tracking of YFP$^+$ adult-born neurons in the olfactory bulb (OB) at 30 days after tamoxifen induction. Bottom: Diagram showing a sagittal section through mouse brain, demonstrating the lateral ventricle (LV), rostral migratory stream (RMS), and OB. (B) Representative images of Nestin-YFP$^+$ neurons co-immunostained with the neuronal marker NeuN (blue) along the RMS and in the OB of WT and fl/fl mice at 30 days after induction. (C) Representative sagittal sections of WT and ADAM10$^{fl/fl}$ Nestin: CreER;Rosa26YFP animals 21 days after tamoxifen injections. Immunostaining for YFP (green) shows the SVZ-RMS-OB route SVZ progenitors take to the OB. Inserts show a high magnification view of the RMS and OB in WT and ADAM10$^{fl/fl}$ mice. (D) Quantification of the data shown in B. 2196 and 1174 WT and ADAM10$^{fl/fl}$ YFP$^+$ cells were quantified in the OB, respectively. YFP$^+$NeuN$^+$ cells in WT *vs.* ADAM10$^{fl/fl}$: 29 ± 1.76/mm^3 *vs.* 15 ± 1.52/mm^3, P = 0.001, respectively. The percentage of newly generated neurons within the YFP population (YFP$^+$NeuN$^+$/total YFP$^+$ cells) was quantified: WT *vs.* ADAM10$^{fl/fl}$: 55.09 ± 2.66% *vs.* 49.21 ± 2.71%, P = 0.2364, respectively. (E) Top: Experimental paradigm. Bottom: Behavioral testing for short-term olfactory memory. Animals presented with the same odor at a short interval, and odor investigation was assessed in WT and ADAM10$^{fl/fl}$ mice at 30- and 60-minute intervals using EthoVision XT9 software (Noldus). Odor investigation in WT group at 30 minutes: ***P = 0.0007, and 1 hour: *P = 0.0380; ADAM10$^{fl/fl}$ group at 30 minutes: P = 0.1678, and 1 hour: P = 0.4679. For C, n = 3, B, D, n = 4, E, n = 16 WT, n = 12 ADAM10$^{fl/fl}$. Students unpaired t-test. Paired t-test in E. Scale bars: 50 µm. Error bars represent the mean ± SEM. ADAM10: A disintegrin and metalloproteinase 10; NeuN: neuronal nuclei; NSC: neural stem cell; SVZ: subventricular zone; OB: olfactory bulb; WT: wild-type; YFP: yellow fluorescent protein.

Using an inducible Nestin promoter, we deleted ADAM10 in both stem and progenitor cells. This technique allowed us to study the roles of ADAM10 locally in the SVZ as stem cells do not function in isolation, rather they interact through direct and indirect mechanisms. Crossing the Nestin::ADAM10$^{fl/fl}$ with a GFAP-GFP mouse line allowed us to focus on the effect of ADAM10 deletion in SVZ cells on the NSCs. Future experiments could focus on YFP$^+$ (Nestin$^+$) cells, with the caveat that progenitor cells would also be targeted.

We identified the apical stem cell marker, JAMC, and its downstream target Rap1Gap as a substrate for ADAM10. This is the first time JAMC was identified as a substrate for ADAM10 in NSCs. Furthermore, RAP1Gap has been implicated in the molecular machinery promoting niche exit in embryonic NSCs (Niola et al., 2012). Here, we similarly identified a previously unreported role for Rap1Gap in the adult SVZ nice. We observed the same increase in WT adult NSCs during differentiation, but reported that deletion of ADAM10 activity prevents the elevation of RAP1Gap, thereby maintaining active GTP bound RAP1, a key mediator of cell adhesion. Moreover, decreased RAP1Gap in ADAM10$^{fl/fl}$ NSCs is rescued by overexpression of JAMC, placing RAP1 activity downstream of ADAM10 initiated JAMC signaling. It is of interest that overexpression of JAMC increased Rap1Gap levels in fl/fl cells more than in WT cells with overexpression. It is possible that the signaling pathway in WT cells is already saturated so that overexpression of JAMC has minimal impact on Rap1Gap levels whereas in ADAM10$^{fl/fl}$ cells the threshold is much higher. Taken together, these findings suggest that ADAM10 regulates a pathway essential for NSC anchorage to the ventricular wall by way of Rap1Gap. Future studies could explore the role of ADAM10 in mediating NSC anchorage specifically to ependymal cells, since if the apical domain is indeed important for maintaining quiescence, adherence to ependymal cells should be relevant as well. It would be of additional interest to explore whether this mechanism is preserved in mouse hippocampal neurogenesis or in the human subependymal zone, the human equivalent to the SVZ, which might have implications for regeneration. It is unclear whether a similar mechanism would be preserved in the adult where distinct differences exist, notably, a hypocellular "gap" zone separating the ependymal layer from a ribbon layer that includes astrocytic processes and proliferating astrocytes (Quinones-Hinojosa et al., 2006). While the architecture is uniquely different, the function appears to be conserved with evidence of migrating chains of cells observed in the non-human primates (Sanai et al., 2011).

Limitations

Two points worth mentioning are limitations with the ADAM10 activator and inhibitor. Previous studies have suggested that all-trans retinoic acid does not increase ADAM17 expression (Endres et al., 2005), however, we cannot rule out that acitretin may have activity against other alpha secretases such as ADAM9 and ADAM17. The ADAM10 inhibitor GI254023X exerts function by chelating the Zn^{2+} of the protease active site and also works on ADAM17, MMP2, and MMP (Dreymueller et al., 2015). Future experiments can explore the effect of the activator and inhibitor on various other proteases.

We should also point out that basal cleavage of JAMC would be expected to occur *in vivo*, but was likely not detected in our experiments due to limitations in the experimental assay sensitivity, because of JAMC low expression and the ability of the cleavage product to diffuse (Hirano et al., 2018).

Conclusion

In summary, we found that deletion of ADAM10 from NSCs of the adult SVZ prevents lineage progression, impairs neurogenesis, and compromises short-term olfactory memory by increasing NSC anchorage to the apical domain. We also identified JAMC, an apical neural stem cell marker, as a substrate for ADAM10 mediated cleavage in the SVZ. Mechanistically, we describe JAMC and its downstream target RAP1Gap (RAP1 GTPase-activating proteins), as downstream effectors of ADAM10, which regulate NSC positioning, cell cycle status, and lineage progression.

Our data demonstrate maintenance of "stemness" and decreased lineage progression following the deletion of ADAM10 in NSCs/NPCs, and suggest that ADAM10 may play a role in the maintenance of NSCs in the niche as opposed to their recruitment to active neurogenesis. It will be interesting to assess if ADAM10 also has a role in symmetrical self-renewal of a neural stem cell using methodology as previously described (Conti et al., 2005). Without ADAM10 activity, RAP1-GTP is high, promoting adhesion and retention in the apical SVZ, while ADAM10 processing of JAMC or RAP1Gap overexpression promotes lineage progression (**Figure 11**). Understanding these basic mechanisms responsible for neural stem cell lineage progression and adhesion is critical in the identification of targets for the development of novel tools to enhance the regenerative capacities of the central nervous system, which can provide therapeutic benefit to patients suffering from a wide variety of pathologic conditions.

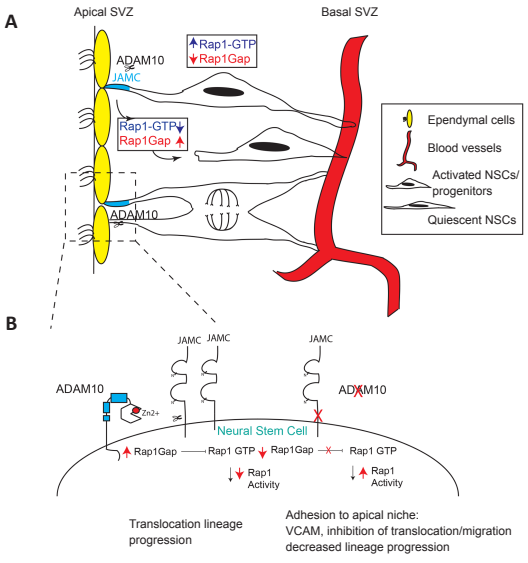

Figure 11 | Summary diagram of the study.
(A) JAMC located at the apical plasma membrane of NSCs is processed by ADAM10. Without ADAM10, RAP1Gap expression is decreased, and RAP1-GTP is high, promoting adhesion and retention in the apical SVZ. ADAM10 processing of JAMC or RAP1Gap over-expression promotes translocation to the basal SVZ. (B) Magnified schematic of the NSC-Niche interaction. ADAM10: A disintegrin and metalloproteinase 10; JAMC: junctional adhesion molecule C; NSC: neural stem cell; SVZ: subventricular zone; VCAM: vascular cell adhesion molecule.

Acknowledgments: *We would like to thank Dr. Dempsey (Department of Pediatrics and Communicable Diseases, University of Michigan) and Dr. Howard Crawford (Department of Cancer Biology, Mayo Clinic Florida, Jacksonville) for providing the ADAM10 mouse line. We would additionally like to thank Dr. Santoso for providing the pcDNA-JAM3 plasmid (Justus-Liebig-University, Giessen, Germany) and members of the Principal Investigators' Tsirka and Aguirre labs for helpful discussions and suggestions.*

Author contributions: *NM and AA devised the experiments. NM, SD, and EX conducted the experiments. NM, GWK, SET, and AA analyzed the data. All authors participated in writing and editing of the manuscript and approved its final version.*

Conflicts of interest: *The authors have no conflicts of interests to report.*

References

Aguirre A, Rubio ME, Gallo V (2010) Notch and EGFR pathway interaction regulates neural stem cell number and self-renewal. Nature 467:323-327.

Aguirre A, Rizvi TA, Ratner N, Gallo V (2005) Overexpression of the epidermal growth factor receptor confers migratory properties to nonmigratory postnatal neural progenitors. J Neurosci 25:11092-11106.

Arenkiel BR (2010) Adult neurogenesis supports short-term olfactory memory. J Neurophysiol 103:2935-2937.

Bos JL, de Bruyn K, Enserink J, Kuiperij B, Rangarajan S, Rehmann H, Riedl J, de Rooij J, van Mansfeld F, Zwartkruis F (2003) The role of Rap1 in integrin-mediated cell adhesion. Biochem Soc Trans 31(Pt 1):83-86.

Brennaman LH, Moss ML, Maness PF (2014) EphrinA/EphA-induced ectodomain shedding of neural cell adhesion molecule regulates growth cone repulsion through ADAM10 metalloprotease. J Neurochem 128:267-279.

Breton-Provencher V, Lemasson M, Peralta MR, 3rd, Saghatelyan A (2009) Interneurons produced in adulthood are required for the normal functioning of the olfactory bulb network and for the execution of selected olfactory behaviors. J Neurosci 29:15245-15257.

Bryn T, Mahic M, Enserink JM, Schwede F, Aandahl EM, Tasken K (2006) The cyclic AMP-Epac1-Rap1 pathway is dissociated from regulation of effector functions in monocytes but acquires immunoregulatory function in mature macrophages. J Immunol 176:7361-7370.

Chen YY, Hehr CL, Atkinson-Leadbeater K, Hocking JC, McFarlane S (2007) Targeting of retinal axons requires the metalloproteinase ADAM10. J Neurosci 27:8448-8456.

Cheung TH, Rando TA (2013) Molecular regulation of stem cell quiescence. Nat Rev Mol Cell Biol 14:329-340.

Conti L, Pollard SM, Gorba T, Reitano E, Toselli M, Biella G, Sun Y, Sanzone S, Ying QL, Cattaneo E, Smith A (2005) Niche-independent symmetrical self-renewal of a mammalian tissue stem cell. PLoS Biol 3:e283.

Doetsch F, Caille I, Lim DA, Garcia-Verdugo JM, Alvarez-Buylla A (1999) Subventricular zone astrocytes are neural stem cells in the adult mammalian brain. Cell 97:703-716.

Doetsch F, Petreanu L, Caille I, Garcia-Verdugo JM, Alvarez-Buylla A (2002) EGF converts transit-amplifying neurogenic precursors in the adult brain into multipotent stem cells. Neuron 36:1021-1034.

Dreymueller D, Uhlig S, Ludwig A (2015) ADAM-family metalloproteinases in lung inflammation: potential therapeutic targets. Am J Physiol Lung Cell Mol Physiol 308:L325-343.

Endres K, Postina R, Schroeder A, Mueller U, Fahrenholz F (2005) Shedding of the amyloid precursor protein-like protein APLP2 by disintegrin-metalloproteinases. FEBS J 272:5808-5820.

Famulski JK, Trivedi N, Howell D, Yang Y, Tong Y, Gilbertson R, Solecki DJ (2010) Siah regulation of Pard3A controls neuronal cell adhesion during germinal zone exit. Science 330:1834-1838.

Franke B, Akkerman JW, Bos JL (1997) Rapid Ca2+-mediated activation of Rap1 in human platelets. EMBO J 16:252-259.

Fuentealba LC, Obernier K, Alvarez-Buylla A (2012) Adult neural stem cells bridge their niche. Cell Stem Cell 10:698-708.

Gattazzo F, Urciuolo A, Bonaldo P (2014) Extracellular matrix: a dynamic microenvironment for stem cell niche. Biochim Biophys Acta 1840:2506-2519.

Graziola F, Colombo E, Tiberio R, Leigheb G, Bozzo C (2017) Mycobacterium ulcerans mycolactone interferes with adhesion, migration and proliferation of primary human keratinocytes and HaCaT cell line. Arch Dermatol Res 309:179-189.

Harrison N, Koo CZ, Tomlinson MG (2021) Regulation of ADAM10 by the TspanC8 family of tetraspanins and their therapeutic potential. Int J Mol Sci 22:6707.

Hartmann D, de Strooper B, Serneels L, Craessaerts K, Herreman A, Annaert W, Umans L, Lubke T, Lena Illert A, von Figura K, Saftig P (2002) The disintegrin/metalloprotease ADAM 10 is essential for Notch signalling but not for alpha-secretase activity in fibroblasts. Hum Mol Genet 11:2615-2624.

Hirano Y, Ode Y, Ochani M, Wang P, Aziz M (2018) Targeting junctional adhesion molecule-C ameliorates sepsis-induced acute lung injury by decreasing CXCR4(+) aged neutrophils. J Leukoc Biol 104:1159-1171.

Holthoewer D, Endres K, Schuck F, Hiemke C, Schmitt U, Fahrenholz F (2012) Acitretin, an enhancer of alpha-secretase expression, crosses the blood-brain barrier and is not eliminated by P-glycoprotein. Neurodegener Dis 10(1-4):224-228.

Janes PW, Saha N, Barton WA, Kolev MV, Wimmer-Kleikamp SH, Nievergall E, Blobel CP, Himanen JP, Lackmann M, Nikolov DB (2005) Adam meets Eph: an ADAM substrate recognition module acts as a molecular switch for ephrin cleavage in trans. Cell 123:291-304.

Johansson CB, Svensson M, Wallstedt L, Janson AM, Frisen J (1999a) Neural stem cells in the adult human brain. Exp Cell Res 253:733-736.

Johansson CB, Momma S, Clarke DL, Risling M, Lendahl U, Frisen J (1999b) Identification of a neural stem cell in the adult mammalian central nervous system. Cell 96:25-34.

Jorissen E, Prox J, Bernreuther C, Weber S, Schwanbeck R, Serneels L, Snellinx A, Craessaerts K, Thathiah A, Tesseur I, Bartsch U, Weskamp G, Blobel CP, Glatzel M, De Strooper B, Saftig P (2010) The disintegrin/metalloproteinase ADAM10 is essential for the establishment of the brain cortex. J Neurosci 30:4833-4844.

Kageyama R, Imayoshi I, Sakamoto M (2012) The role of neurogenesis in olfaction-dependent behaviors. Behav Brain Res 227:459-463.

Kerever A, Schnack J, Vellinga D, Ichikawa N, Moon C, Arikawa-Hirasawa E, Efird JT, Mercier F (2007) Novel extracellular matrix structures in the neural stem cell niche capture the neurogenic factor fibroblast growth factor 2 from the extracellular milieu. Stem Cells 25:2146-2157.

Klingener M, Chavali M, Singh J, McMillan N, Coomes A, Dempsey PJ, Chen EI, Aguirre A (2014) N-cadherin promotes recruitment and migration of neural progenitor cells from the SVZ neural stem cell niche into demyelinated lesions. J Neurosci 34:9590-9606.

Kokovay E, Wang Y, Kusek G, Wurster R, Lederman P, Lowry N, Shen Q, Temple S (2012) VCAM1 is essential to maintain the structure of the SVZ niche and acts as an environmental sensor to regulate SVZ lineage progression. Cell Stem Cell 11:220-230.

Kokovay E, Goderie S, Wang Y, Lotz S, Lin G, Sun Y, Roysam B, Shen Q, Temple S (2010) Adult SVZ lineage cells home to and leave the vascular niche via differential responses to SDF1/CXCR4 signaling. Cell Stem Cell 7:163-173.

Krishnaswamy VR, Korrapati PS (2014) Role of dermatopontin in re-epithelialization: implications on keratinocyte migration and proliferation. Sci Rep 4:7385.

Lathia JD, Rao MS, Mattson MP, Ffrench-Constant C (2007) The microenvironment of the embryonic neural stem cell: lessons from adult niches? Dev Dyn 236:3267-3282.

Li X, Stankovic M, Lee BP, Aurrand-Lions M, Hahn CN, Lu Y, Imhof BA, Vadas MA, Gamble JR (2009) JAM-C induces endothelial cell permeability through its association and regulation of {beta}3 integrins. Arterioscler Thromb Vasc Biol 29:1200-1206.

Liang CC, Park AY, Guan JL (2007) In vitro scratch assay: a convenient and inexpensive method for analysis of cell migration in vitro. Nat Protoc 2:329-333.

Lois C, Alvarez-Buylla A (1993) Proliferating subventricular zone cells in the adult mammalian forebrain can differentiate into neurons and glia. Proc Natl Acad Sci U S A 90:2074-2077.

Loulier K, Lathia JD, Marthiens V, Relucio J, Mughal MR, Tang SC, Coksaygan T, Hall PE, Chigurupati S, Patton B, Colognato H, Rao MS, Mattson MP, Haydar TF, Ffrench-Constant C (2009) beta1 integrin maintains integrity of the embryonic neocortical stem cell niche. PLoS Biol 7:e1000176.

Ming G, Song H (2011) Adult neurogenesis in the mammalian brain: significant answers and significant questions. Neuron 70:687-702.

Moreno MM, Linster C, Escanilla O, Sacquet J, Didier A, Mandairon N (2009) Olfactory perceptual learning requires adult neurogenesis. Proc Natl Acad Sci U S A 106:17980-17985.

Niola F, Zhao X, Singh D, Castano A, Sullivan R, Lauria M, Nam HS, Zhuang Y, Benezra R, Di Bernardo D, Iavarone A, Lasorella A (2012) Id proteins synchronize stemness and anchorage to the niche of neural stem cells. Nat Cell Biol 14:477-487.

Orlova VV, Economopoulou M, Lupu F, Santoso S, Chavakis T (2006) Junctional adhesion molecule-C regulates vascular endothelial permeability by modulating VE-cadherin-mediated cell-cell contacts. J Exp Med 203:2703-2714.

Pan Y et al. (2021) NF1 mutation drives neuronal activity-dependent initiation of optic glioma. Nature 594:277-282.

Porlan E, Marti-Prado B, Morante-Redolat JM, Consiglio A, Delgado AC, Kypta R, Lopez-Otin C, Kirstein M, Farinas I (2014) MT5-MMP regulates adult neural stem cell functional quiescence through the cleavage of N-cadherin. Nat Cell Biol 16:629-638.

Quinones-Hinojosa A, Sanai N, Soriano-Navarro M, Gonzalez-Perez O, Mirzadeh Z, Gil-Perotin S, Romero-Rodriguez R, Berger MS, Garcia-Verdugo JM, Alvarez-Buylla A (2006) Cellular composition and cytoarchitecture of the adult human subventricular zone: a niche of neural stem cells. J Comp Neurol 494:415-434.

Rabquer BJ, Amin MA, Teegala N, Shaheen MK, Tsou PS, Ruth JH, Lesch CA, Imhof BA, Koch AE (2010) Junctional adhesion molecule-C is a soluble mediator of angiogenesis. J Immunol 185:1777-1785.

Reiss K, Maretzky T, Ludwig A, Tousseyn T, de Strooper B, Hartmann D, Saftig P (2005) ADAM10 cleavage of N-cadherin and regulation of cell-cell adhesion and beta-catenin nuclear signalling. EMBO J 24:742-752.

Reynolds BA, Weiss S (1992) Generation of neurons and astrocytes from isolated cells of the adult mammalian central nervous system. Science 255:1707-1710.

Saftig P, Lichtenthaler SF (2015) The alpha secretase ADAM10: A metalloprotease with multiple functions in the brain. Prog Neurobiol 135:1-20.

Santoso S, Sachs UJH, Kroll H, Linder M, Ruf A, Preissner KT, Chavakis T (2002) The junctional adhesion molecule 3 (JAM-3) on human platelets is a counterreceptor for the leukocyte integrin Mac-1. J Exp Med 196:679-691.

Schneider CA, Rasband WS, Eliceiri KW (2012) NIH Image to ImageJ: 25 years of image analysis. Nat Methods 9:671-675.

Sanai N, Nguyen T, Ihrie RA, Mirzadeh Z, Tsai HH, Wong M, Gupta N, Berger MS, Huang E, Garcia-Verdugo JM, Rowitch DH, Alvarez-Buylla A (2011) Corridors of migrating neurons in the human brain and their decline during infancy. Nature 478:382-386.

Shen Q, Wang Y, Kokovay E, Lin G, Chuang SM, Goderie SK, Roysam B, Temple S (2008) Adult SVZ stem cells lie in a vascular niche: a quantitative analysis of niche cell-cell interactions. Cell Stem Cell 3:289-300.

Solanas G, Cortina C, Sevillano M, Batlle E (2011) Cleavage of E-cadherin by ADAM10 mediates epithelial cell sorting downstream of EphB signalling. Nat Cell Biol 13:1100-1107.

Stelzer S, Worlitzer MM, Bahnassawy L, Hemmer K, Rugani K, Werthschulte I, Schon AL, Brinkmann BF, Bunk EC, Palm T, Ebnet K, Schwamborn JC (2012) JAM-C is an apical surface marker for neural stem cells. Stem Cells Dev 21:757-766.

Tippmann F, Hundt J, Schneider A, Endres K, Fahrenholz F (2009) Up-regulation of the alpha-secretase ADAM10 by retinoic acid receptors and acitretin. FASEB J 23:1643-1654.

Tsai YH, VanDussen KL, Sawey ET, Wade AW, Kasper C, Rakshit S, Bhatt RG, Stoeck A, Maillard I, Crawford HC, Samuelson LC, Dempsey PJ (2014) ADAM10 regulates Notch function in intestinal stem cells of mice. Gastroenterology 147:822-834.e813.

Wang W, Lu S, Li T, Pan YW, Zou J, Abel GM, Xu L, Storm DR, Xia Z (2015) Inducible activation of ERK5 MAP kinase enhances adult neurogenesis in the olfactory bulb and improves olfactory function. The J Neurosci 35:7833-7849.

Wen C, Metzstein MM, Greenwald I (1997) SUP-17, a Caenorhabditis elegans ADAM protein related to Drosophila KUZBANIAN, and its role in LIN-12/NOTCH signalling. Development 124:4759-4767.

Zhang X, Hei Y, Bai W, Huang T, Kang E, Chen H, Kong C, Yang Y, Ye Y, He X (2020) Toll-like receptor 2 attenuates traumatic brain injury-induced neural stem cell proliferation in dentate gyrus of rats. Neural Plast 2020:9814978.

Zhao C, Deng W, Gage FH (2008) Mechanisms and functional implications of adult neurogenesis. Cell 132:645-660.

Zhu Y, Huang R, Wu Z, Song S, Cheng L, Zhu R (2021) Deep learning-based predictive identification of neural stem cell differentiation. Nat Commun 12:2614.

C-Editor: Zhao M; S-Editor: Li CH; L-Editor: Song LP; T-Editor: Jia Y